Structure-guided Design of Conformationally-constrained Cyclohexane Inhibitors of SARS-CoV-2 3CL Protease

Chamandi S. Dampalla[1], Yunjeong Kim[2], Naemi Bickmeier[2], Athri D. Rathnayake[1], Harry Nhat Nguyen[1], Jian Zheng[3], Maithri M. Kashipathy[4], Matthew A. Baird[1], Kevin P. Battaile[5], Scott Lovell,[4] Stanley Perlman[3], Kyeong-Ok Chang,[2*] William C. Groutas,[1*]

[1]Department of Chemistry, Wichita State University, Wichita, Kansas 67260, USA

[2]Department of Diagnostic Medicine & Pathobiology, College of Veterinary Medicine, Kansas State University, Manhattan, Kansas 66506, USA

[3]Department of Microbiology and Immunology, Carver College of Medicine, University of Iowa, Iowa City, IA 52242, USA

[4]Protein Structure Laboratory, The University of Kansas, Lawrence, Kansas 66047, USA

[5] NYX, New York Structural Biology Center, Upton, NY 11973, USA

*authors to whom correspondence should be addressed.

[1]Department of Chemistry, Wichita State University, Wichita, KS 67260
Tel. (316) 978 7374
e-mail: bill.groutas@wichita.edu

[2]Department of Diagnostic Medicine & Pathobiology, College of Veterinary Medicine, Kansas State University, Manhattan, KS 66506
Tel. (785) 532 3849
e-mail: kchang@vet.ksu.edu

Abstract

A series of non-deuterated and deuterated dipeptidyl aldehyde and masked aldehyde inhibitors that incorporate in their structure a conformationally-constrained cyclohexane moiety was synthesized and found to potently inhibit SARS-CoV-2 3CL protease in biochemical and cell-based assays. Several of the inhibitors were also found to be nanomolar inhibitors of MERS-CoV 3CL protease. The corresponding latent aldehyde bisulfite adducts were found to be equipotent to the precursor aldehydes. High-resolution cocrystal structures confirmed the mechanism of action and illuminated the structural determinants involved in binding. The spatial disposition of the compounds disclosed herein provides an effective means of accessing new chemical space and optimizing pharmacological activity. The cellular permeability of the identified inhibitors and lack of cytotoxicity warrants their advancement as potential therapeutics for COVID-19.
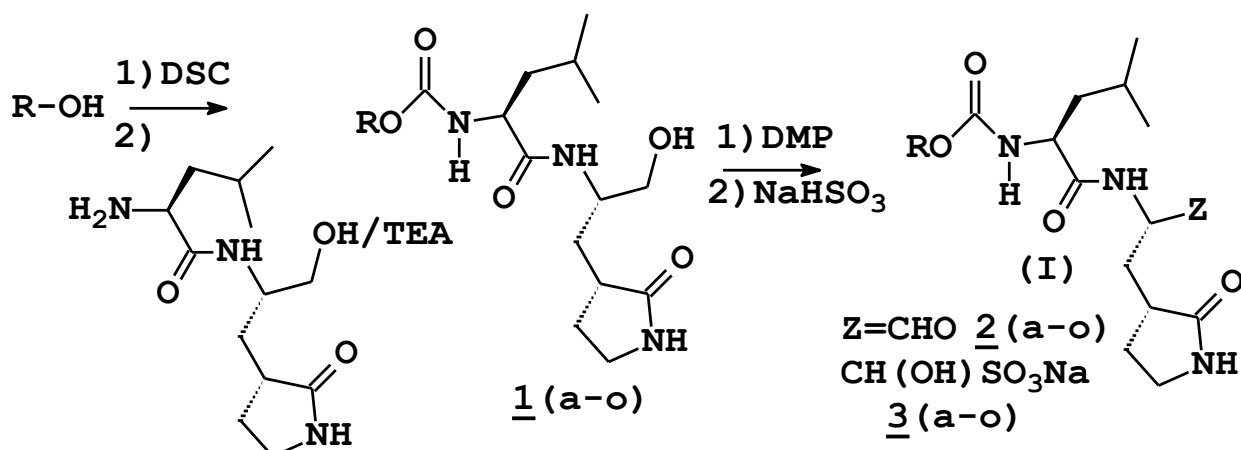
Introduction

Coronaviruses are enveloped, positive-sense, single-stranded RNA viruses that belong to the family *Coronaviridae.*[1] Among human coronaviruses, several strains (229E, NL63, OC43, and KHU1) are the cause of mild upper respiratory infections; however, a few coronaviruses have emerged from animals that cause severe respiratory disease, including Severe Acute Respiratory Syndrome Coronavirus (SARS-CoV), Middle East Respiratory Syndrome Coronavirus (MERS-CoV) and Severe Acute Respiratory Syndrome Coronavirus-2 (SARS-CoV-2).[2] Of particular concern is SARS-CoV-2, the highly pathogenic causative agent of COVID-19 which is associated with high infectivity and is a significant threat to public health worldwide.[3-4] The problem is further compounded by the current lack of effective vaccines or small molecule therapeutics for the treatment of SARS-CoV-2 infections, underscoring the urgent and dire need for the development of prophylactic and therapeutic countermeasures to combat infections by pathogenic coronaviruses.[5-7]

The SARS-CoV-2 genome is large (~30 kb) and similar to the genomes of SARS-CoV and MERS-CoV (~80% and ~50% sequence identity, respectively). It contains two open reading frames (ORF1a and ORF1b) and encodes multiple structural and nonstructural proteins.[1] Translation of the genomic mRNA of ORF1a yields a polyprotein (pp1a), while a second polyprotein (pp1ab) is the product of a ribosomal frameshift that joins ORF1a together with ORF1b. The two polyproteins are processed by a 3C-like protease (3CLpro, also referred to as Main protease, M^{pro}) (11 cleavage sites) and a papain-like cysteine protease (PLpro), resulting in 16 mature nonstructural proteins which

are involved in the replication-transcription complex. The two proteases are essential for viral replication, making them attractive targets for therapeutic intervention.[8-15]

SARS-CoV-2 3CLpro is a homodimer with a catalytic Cys-His dyad (Cys[145]-His[41]) and an extended binding cleft. Substrate specificity profiling studies[12-13] have shown that the protease displays a strong preference for a -Y-Z-Leu-Gln-X sequence, where X is a small amino acid, Y is a hydrophobic amino acid, and Z is solvent-exposed and fairly diverse (V/T/K), corresponding to the amino acid residues -P_4-P_3-P_2-P_1-P_1'- of a substrate or inhibitor.[16] Cleavage is at the P_1-P_1' scissile bond. The 3D structure of SARS-CoV-2 3CLpro is similar to that of SARS-CoV 3CLpro, however, the S_2 subsite of SARS-CoV-2 3CLpro displays considerable plasticity and can accommodate natural and unnatural amino acids with smaller side chains.[12] Similarly, the active site topography of MERS-CoV 3CLpro closely resembles that of SARS-CoV-2 3CLpro.[17] High-resolution crystal structures with bound inhibitors have been determined, enabling the use of structure-guided approaches in the design of inhibitors. In continuing our foray in this area,[17-19] we report herein the results of preliminary studies related to the inhibition of SARS-CoV-2 protease by a series of inhibitors (I) (Scheme 1) that incorporate in their structure a conformationally-constrained cyclohexane moiety envisaged to exploit new chemical space and to optimally engage in favorable binding interactions with the active site of the protease. Furthermore, several deuterated variants of inhibitor (I) were also synthesized to potentially improve the PK properties and ancillary parameters of the inhibitors.[20-22]

<u>**Scheme 1**</u> **Synthesis of inhibitors 2(a-o) and 3(a-o)**

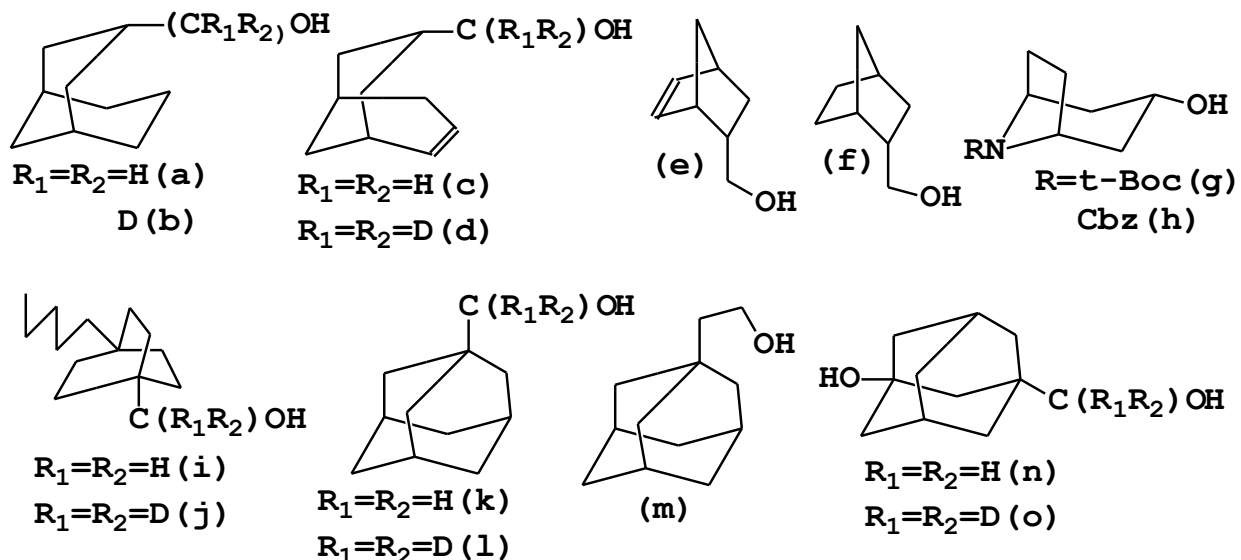## Results and Discussion

Inhibitor Design Rationale

The design of inhibitor (I) (Scheme 1) included the use of a P_1 glutamine surrogate residue and a P_2 Leu residue as recognition elements congruent with the substrate specificity of the protease,[12-13] as well as an aldehyde warhead or a latent aldehyde bisulfite adduct. The design of inhibitor (I) was further abetted by insights gained from examining the available X-ray crystal structures of the protease with inhibitors[12-13,17] and the results of recent studies with cyclohexyl-derived inhibitors with demonstrated efficacy in a mouse model of MERS-CoV-2 infection and potent inhibition against SARS-CoV-2 3CL protease.[17]

Chemistry

The synthesis of inhibitors *2(a-o)* and *3(a-o)* was readily accomplished by activating the precursor primary or secondary alcohol inputs (Scheme 2) with N,N'-disuccinimidyl carbonate (DSC)[23] and coupling the mixed carbonate with the readily-accessible Leu-Gln

surrogate amino alcohol to yield alcohol product *1* which was oxidized with Dess-Martin periodinane (DMP) to generate the corresponding aldehyde (Scheme 1, Z=CHO *2*). The aldehydes were subsequently converted to the corresponding bisulfite adducts (Scheme 1, Z=CH(OH)SO$_3$Na *3*).[24]

Scheme 2 Alcohol inputs (a-o)

$-(CR_1R_2)OH$

$R_1=R_2=H(a)$
$D(b)$

$-C(R_1R_2)OH$

$R_1=R_2=H(c)$
$R_1=R_2=D(d)$

(e) OH

(f) OH

RN OH
$R=t-Boc(g)$
Cbz(h)

$C(R_1R_2)OH$
$R_1=R_2=H(i)$
$R_1=R_2=D(j)$

$C(R_1R_2)OH$
$R_1=R_2=H(k)$
$R_1=R_2=D(l)$

OH
(m)

HO $C(R_1R_2)OH$
$R_1=R_2=H(n)$
$R_1=R_2=D(o)$

Biochemical Studies

The inhibitory activity of compounds *2-3 (a-o)* against SARS-CoV-2 3CL protease[17,25] and their activity in a cell-based system, were determined as described in the experimental section. The IC$_{50}$ values, EC$_{50}$ values for two representative inhibitors (*2a/3a*), and the CC$_{50}$ values in Huh-7, CRFK, or CCL1 cells[17,25] are summarized in Table 1 and they are the average of at least two determinations. The inhibitory activity of compounds *2a/3a*, *2f/3f*, and *2k/3k* against MERS-CoV 3CL protease was also determined as described previously[17-18, 25] and the IC$_{50}$ values are listed in Table 2.

Table 1. IC$_{50}$ and CC$_{50}$ values of SARS-CoV-2 3CLpro inhibitors *2-3(a-o)*

Compound	IC$_{50}$ (µM)	CC$_{50}$ (µM)	Compound	IC$_{50}$ (µM)	CC$_{50}$ (µM)
2a	0.18±0.03[a]	> 100	*3h*	0.37±0.03	> 100
3a	0.17±0.02[a]	> 100	*2i*	0.27±0.02	21±1
2b	0.29±0.05	> 100	*3i*	0.30±0.02	21±3
3b	0.29±0.01	> 100	*2j*	0.31±0.03	20±3
2c	0.31±0.06	> 100	*3j*	0.31±0.06	23±1
3c	0.26±0.05	> 100	*2k*	0.18±0.04	> 100
2d	0.28±0.08	> 100	*3k*	0.15±0.04	> 100
3d	0.30±0.03	> 100	*2l*	0.29±0.04	> 100
2e	0.26±0.05	> 100	*3l*	0.27±0.04	> 100
3e	0.28±0.03	> 100	*2m*	0.27±0.02	> 100
2f	0.14±0.02	> 100	*3m*	0.25±0.04	> 100
3f	0.10±0.01	> 100	*2n*	0.82±0.19	> 100
2g	1.90±0.14	> 100	*3n*	1.03±0.24	> 100
3g	1.71±0.16	> 100	*2o*	0.74±0.26	> 100
2h	0.39±0.02	> 100	*3o*	0.78±0.18	> 100

[a] The EC$_{50}$ values for inhibitors *2a* and *3a* against SARS-CoV-2 in Vero E6 cells were 0.035±0.001 and 0.032±0.001 µM, respectively.

Table 2. IC$_{50}$ values of MERS-CoV 3CLpro inhibitors *2a/3a*, *2f/3f* and *2k/3k*.

Compound	IC$_{50}$ (µM)
2a	0.052±0.001
3a	0.049±0.002
2f	0.063±0.003
3f	0.058±0.002

2k	0.055±0.002
3k	0.053±0.003

It is clearly evident from the results shown in Table 1 that the synthesized compounds display high potency in biochemical assays, with most IC_{50} values in the sub-micromolar range. Furthermore, the inhibitors were found to be devoid of cytotoxicity and the Safety Index (SI), defined as the CC_{50}/IC_{50} ratio, ranged between ~78 to 1110. The potency of deuterated variants **2b/3b** decreased ~1.6-fold (aldehydes) and ~1.7-fold (bisulfite adducts) as compared to the respective non-deuterated compounds **2a/3a** and remained essentially the same in the case of non-deuterated **2n/3n** and deuterated **2o/3o** inhibitors, respectively. A change in geometry from a cyclohexene (**2e/3e**) to a cyclohexane (**2f/3f**) resulted in a 2 to 3-fold increase in potency. The ~5-fold decrease in potency of compounds **2n/3n** compared to **2k/3k** presumably reflects the inimical effect on potency of the 3° hydroxyl group. Importantly, the EC_{50} values of two representative inhibitors (**2a/3a**) against SARS-CoV-2 in Vero E6 cells were found to be ~4.6-fold lower (EC_{50} 0.035 and 0.032 µM, respectively) than the corresponding IC_{50} values, and the selectivity indices of compounds **2a/3a** were very high (2857 and 3125, respectively). The significance of these findings was further augmented by the notable inhibition of MERS-CoV 3CL protease by a select number of inhibitors (Table 2, compounds **2a/3a**, **2f/3f** and **2k/3k**), demonstrating the broad spectrum of antiviral activity displayed by this series of compounds.

Emergence of viral resistance to antiviral drugs is a major concern. We previously reported that GC376 has a high barrier to resistance to feline infectious peritonitis virus (FIPV) in cell culture and naturally infected animals with long term treatment[18]. We also

examined several compounds similar to the series in this report for emergence of viral resistance by serial passaging FIPV in the presence of each compound in cell culture. The EC_{50} values of the compounds did not increase at up to 10 passage number, and the 3CLpro of viruses passaged with each compound has the same sequence as mock-passaged viruses. These results suggest that this series of compounds have a high barrier to resistance.

X-ray Crystallography Studies

In order to elucidate the mechanism of action of the inhibitors as well as identify the structural determinants associated with the binding of inhibitors to the active site of SARS-CoV-2 3CL protease, high-resolution cocrystal structures were determined for inhibitors **2a** and its deuterated analog **3b**, **2f**, **2k**, **3c** and its deuterated analog **3d** and **3e**. The structure of SARS-CoV-2 3CLpro in complex with compound **2a** contained prominent difference electron density consistent with the inhibitor covalently bound to Cys 145 in each subunit (**Figure 1 A** and **B**). The electron density was consistent with the inhibitor aldehyde carbon covalently bound to the Sγ atom of the catalytic Cys145 residue and the formation of a tetrahedral hemithioacetal, confirming the mechanism of action. Both the R and S-enantiomers were observed at the newly formed stereocenter and each enantiomer was modeled with 0.5 occupancy and was observed for all structures described here. Interestingly, **2a** adopts two conformations in which the bicyclic ring is projected away from the S_4 subsite in subunit A and is positioned in the S_4 pocket in subunit B. The inhibitor engages in multiple favorable binding interactions with the enzyme, including direct hydrogen bond interactions with His163 and Glu166 (γ-lactam C=O and N-H, respectively), His41, Phe 140, Ser144, His164, and Gln189 (**Figure 1 C**

9

and **D**). The isobutyl side chain of Leu is ensconced in the hydrophobic S_2 pocket and the

γ-lactam ring of the P_1 Gln surrogate is nestled in the S_1 subsite forming hydrogen bonds

with His163 and Glu166. In addition, the lipophilic bicyclic ring in subunit A is directed

towards the surface whereas in subunit B is anchored in the vicinity of the hydrophobic

S_4 pocket that is lined by Ala191, Leu197, and Pro168 (**Figure 1 E** and **F**). It should be

noted that the eleven sites in the pp1a and pp1ab polyproteins cleaved by the protease

are all characterized by the presence of a P_1 Gln residue, which is conserved in all known

coronavirus 3CLpro cleavage sites. Interestingly, the deuterated analog **3b** adopts the

same binding mode and superimposes nearly identical to **2a** as shown in **Figure S1**. The

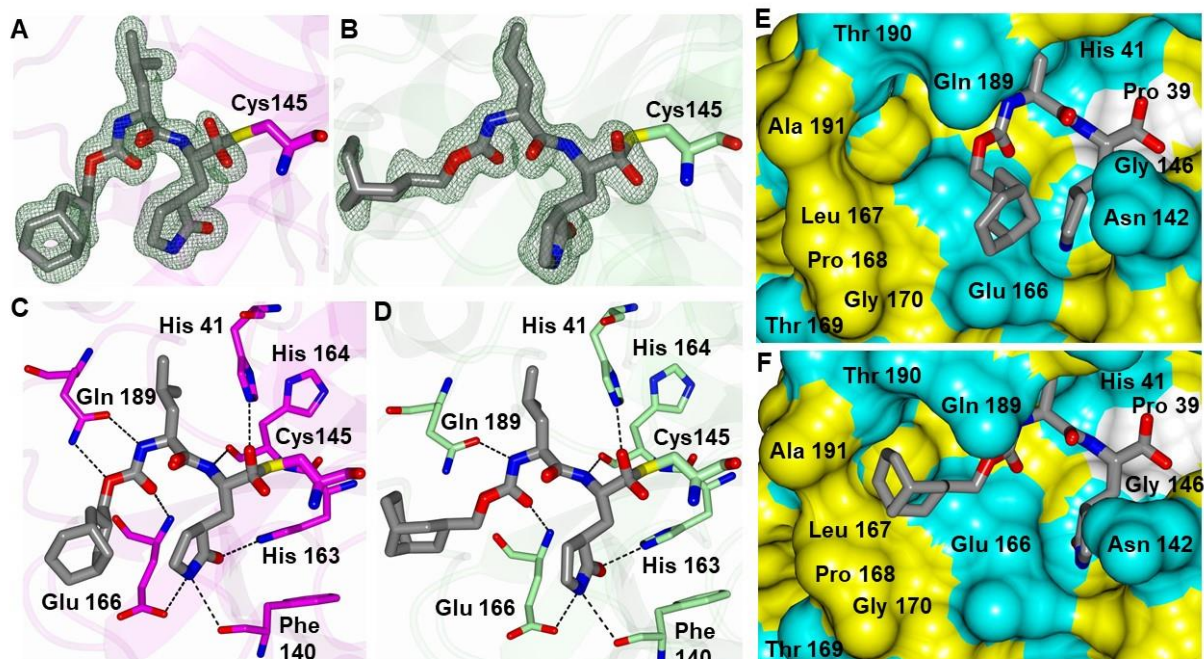RMSD deviation between the Cα atoms of **2a** and **3b** was 0.27 Å for 594 residues aligned.

Figure 1. Binding mode of *2a* (gray) with SARS-CoV-2 3CLpro associated with subunit A (**A, C**) and subunit B (**B, D**). Fo-Fc Polder omit map (green mesh) contoured at 3σ (**A, B**). Hydrogen bond interactions (dashed lines) (**C, D**). Surface representations showing the orientation of *2a* in subunit A (**E**) and subunit B (**F**) near the S_4 subsite of SARS2 3CLpro with neighboring residues colored yellow (nonpolar), cyan (polar), and white (weakly polar).

Likewise, the structure of *3c* shows similar binding mode properties as observed for *2a* (**Figure 2 A**, **C** and **E**). The inhibitor engages in multiple favorable binding interactions with the enzyme, including direct hydrogen bond interactions with His163 and Glu166 (γ-lactam C=O and N-H, respectively), His41, Ser144, His164, and Gln189. The bicyclic ring is oriented within the hydrophobic S_4 pocket, in both subunits. Likewise, the structure of SARS-CoV-2 3CL protease with deuterated inhibitor *3d* adopts a very similar binding mode (**Figure 2 C, D, F**). The main difference is that the electron density for *3c* is most consistent with an axial conformation of the carbon atom attached to the bicyclic

ring whereas *3d* appears to adopt an equatorial orientation (**Figure S2**). The structures are very similar overall and the superposition yielded an RMSD deviation between the Cα atoms of 0.25 Å for 596 residues aligned.
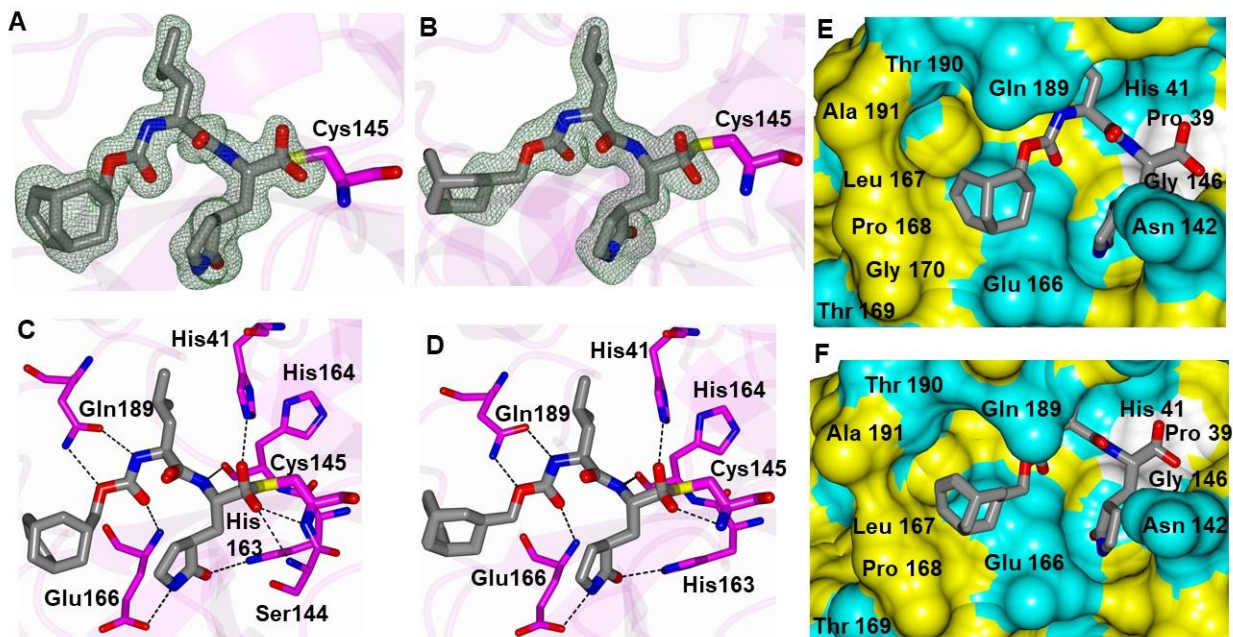

Figure 2. Binding mode of *3c* (**A, B, E**) and its deuterated analog *3d* (**C, D, F**) with SARS-CoV-2 3CLpro. Fo-Fc Polder omit map (green mesh) contoured at 3σ (**A, B**). Hydrogen bond interactions (dashed lines) (**C, D**). **E/F**: Surface representation showing the orientation of *3c* (**E**) and *3d* (**F**) near the S$_4$ subsite of SARS-CoV-2 3CLpro with neighboring residues colored yellow (nonpolar), cyan (polar), and white (weakly polar).

Similarly, inhibitors *2f*, *2k* and *3e* in complex with SARS-CoV-2 were found to adopt similar binding modes in the active site of the protease as shown in **Figure 3** and **Figure S3**. Collectively, the bicyclic rings of the inhibitors span a relatively small region in the active site and cover a space of approximately 6.3 Å (**Figure 4**). As such, these cocrystal structures provide valuable insights for further structure-guided multiparameter optimization.
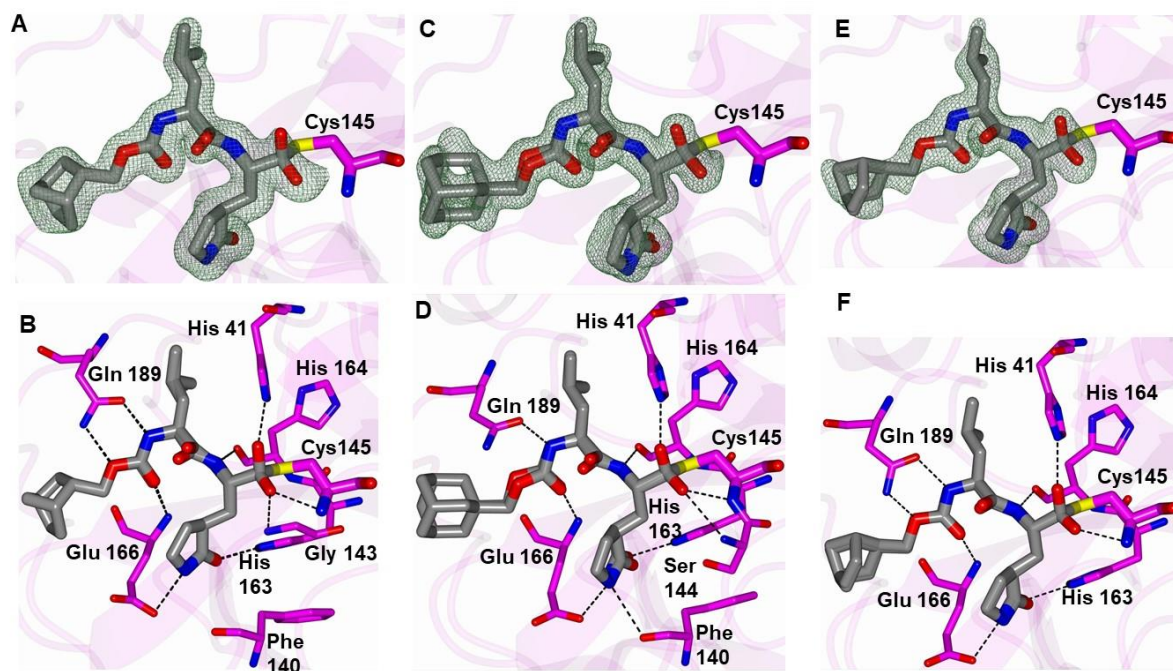
Figure 3. Binding mode of **2f** (**A, B**), **2k** (**C, D**) and **3e** (**E, F**) with SARS2-CoV-2 3CLpro. Fo-Fc Polder omit map (green mesh) contoured at 3σ (**A, C, E**). Hydrogen bond interactions (dashed lines) (**B, D, F**).
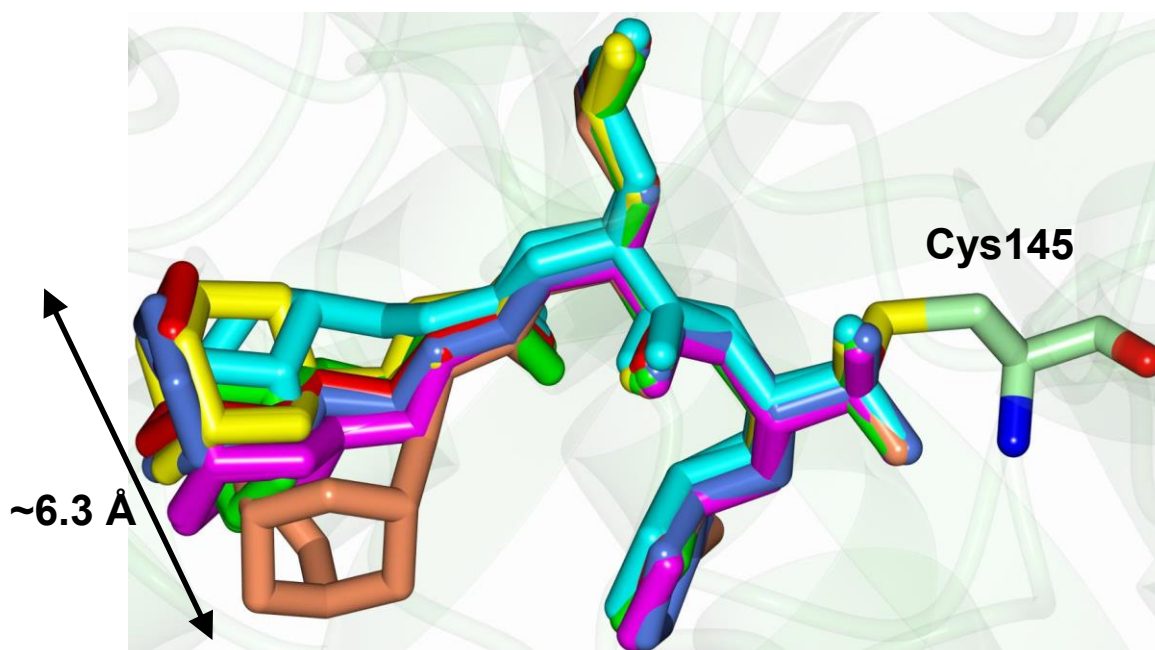
Figure 4. Superposition of all seven inhibitor bound structures *2a* (red), *3b* (blue), *2f* (cyan), *2k* (yellow), *3c* (coral), *3d* (magenta) and *3e* (green). The bicyclic rings cover a space of approximately 6.3 Å in the S_4 subsite.

Conclusions

Given the major clinical importance associated with the SARS-CoV-2 pandemic and the current paucity of effective countermeasures, the results of the studies described herein can serve as a launching pad for conducting further pre-clinical studies. Most of the compounds exhibited high potency in biochemical assays and, for two of the compounds tested, in cellular assays. Furthermore, members of this series were also found to potently inhibit MERS-CoV 3CL protease, suggesting that the compounds can be developed into broad-spectrum antivirals. Since there are no known human proteases that have a primary substrate specificity P_1 residue that is Gln, these inhibitors could also display high selectivity and diminished off-target effects. Furthermore, the utilization of an aldehyde warhead, or a latent aldehyde functionality that can rapidly generate the aldehyde *in vivo*, in the design of transition state inhibitors is advantageous for several reasons, including rapid engagement with the target leading to the *reversible* formation of a covalent adduct. The high reactivity of aldehydes is generally viewed as a toxicity alert, however, the safety indices for most of the compounds reported herein were found to be high. Indeed, a number of pharmaceuticals that incorporate in their structure an aldehyde functionality are currently in clinical use and, furthermore, toxicity arising from the presence of the aldehyde is context-specific,[26] as is presumably the case here. Finally, the present study also sought to exploit the kinetic isotope effect associated with the H/D bioisosteric replacement[27-28] in order to dampen oxidative metabolism at the -CH_2O-

metabolic soft spot in the inhibitors,[29] as well as to reduce toxicity. Thus, the availability of equipotent deuterated analogs that display improved PK characteristics enhances further the significance of the results reported herein. Evaluation of a select number of inhibitors in a mouse model of SARS-CoV-2 infection is in progress and the results will be reported in due course. In conclusion, a series of potent transition state inhibitors of SARS-CoV-2 3CL protease that incorporate in their structures a conformationally-constrained cyclohexyl moiety is reported.

Experimental section

General

Reagents and dry solvents were purchased from various chemical suppliers (Sigma-Aldrich, Acros Organics, Chem-Impex, TCI America, Oakwood chemical, APExBIO, Cambridge Isotopes, Alpha Aesar, Fisher and Advanced Chemblocks) and were used as obtained. Silica gel (230-450 mesh) used for flash chromatography was purchased from Sorbent Technologies (Atlanta, GA). Thin layer chromatography was performed using Analtech silica gel plates. Visualization was accomplished using UV light and/or iodine. NMR spectra were recorded in $CDCl_3$ or DMSO-d_6 using Varian XL-400 spectrometer. Melting points were recorded on a Mel-Temp apparatus and are uncorrected. High resolution mass spectrometry (HRMS) was performed at the Wichita State University Mass Spectrometry lab using Orbitrap Velos Pro mass spectrometer (ThermoFisher, Waltham, MA) equipped with an electrospray ion source. The purity of all final compounds was >95% as evidenced by NMR analysis.

Synthesis of compounds

Preparation of compounds *1(a-o)*. General procedure. To a solution of alcohol (1 eq) (Scheme 2) in anhydrous acetonitrile (10 mL/g alcohol) was added N,N'-disuccinimidyl carbonate (1.2 eq) and TEA (3.0 eq) and the reaction mixture was stirred for 4h at room temperature. The solvent was removed *in vacuo* and the residue was dissolved in ethyl acetate (40 mL/g alcohol). The organic phase was washed with saturated aqueous $NaHCO_3$ (2 x 20 mL/ g alcohol), followed by brine (20 mL/ g alcohol). The organic layers were combined and dried over anhydrous Na_2SO_4, filtered and concentrated *in vacuo* to yield the mixed carbonate which was used in the next step without further purification.

To a solution of Leu-Gln surrogate amino alcohol (1.0 eq) in dry methylene chloride (10 mL/g of amino alcohol) was added TEA (1.5 eq) and the reaction mixture was stirred for 20 min at room temperature (solution 1). In a separate flask, the mixed carbonate was dissolved in dry methylene chloride (10 mL/g of carbonate) (solution 2). Solution 1 was added to solution 2 and the reaction mixture was stirred 3h at room temperature. Methylene chloride was added to the organic phase (40 mL/g of carbonate) and then washed with saturated aqueous $NaHCO_3$ (2 x 20 mL/ g alcohol), followed by brine (20 mL/ g alcohol). The organic phase was dried over anhydrous Na_2SO_4, filtered and concentrated *in vacuo*. The resultant crude product was purified by flash chromatography (hexane/ethyl acetate) to yield dipeptidyl alcohol *1* as a white solid.

((1R,5S)-Bicyclo[3.3.1]nonan-3-yl)methyl ((S)-1-(((S)-1-hydroxy-3-((S)-2-oxopyrrolidin-3-yl)propan-2-yl)amino)-4-methyl-1-oxopentan-2-yl)carbamate (*1a*). Yield (35%); ^{1}H NMR (400 MHz, CDCl$_3$) δ 7.75 (d, *J* = 7.2 Hz, 1H), 6.24 (s, 1H), 5.31 (d, *J* = 9.1 Hz, 1H), 4.29 – 4.10 (m, 1H), 4.10 – 3.93 (m, 1H), 3.89 (d, *J* = 6.3 Hz, 1H), 3.71 – 3.54 (m, 2H), 3.48 (d, *J* = 2.0 Hz, 1H), 3.39 – 3.27 (m, 2H), 2.55 – 2.25 (m, 3H), 2.03 (d, *J* = 11.9 Hz,

3H), 1.96 – 1.77 (m, 4H), 1.77 – 1.57 (m, 4H), 1.57 – 1.44 (m, 1H), 1.37 (d, J = 9.5 Hz, 4H), 1.27 – 1.15 (m, 1H), 1.09 (dd, J = 12.8, 2.6 Hz, 1H), 0.95 (d, J = 6.3 Hz, 6H), 0.91 – 0.80 (m, 2H).

((1R,3S,5S)-Bicyclo[3.3.1]nonan-3-yl)methyl-d2 ((S)-1-(((S)-1-hydroxy-3-((S)-2-oxopyrrolidin-3-yl)propan-2-yl)amino)-4-methyl-1-oxopentan-2-yl)carbamate (*1b*). Yield (36%); ^{1}H NMR (400 MHz, CDCl₃) δ 7.77 (d, J = 7.1 Hz, 1H), 6.25 (s, 1H), 5.30 (s, 1H), 4.27 – 3.93 (m, 2H), 3.69 – 3.55 (m, 2H), 3.39 – 3.32 (m, 2H), 2.53 – 2.35 (m, 2H), 2.09 – 1.96 (m, 4H), 1.96 – 1.77 (m, 3H), 1.77 – 1.58 (m, 5H), 1.58 – 1.47 (m, 1H), 1.45 – 1.30 (m, 5H), 1.09 (d, J = 12.8 Hz, 1H), 0.95 (d, J = 6.4 Hz, 6H), 0.88 (d, J = 13.1 Hz, 2H).

((1S,5R)-Bicyclo[3.3.1]non-6-en-3-yl)methyl((S)-1-(((S)-1-hydroxy-3-((S)-2-oxopyrrolidin-3-yl)propan-2-yl)amino)-4-methyl-1-oxopentan-2-yl)carbamate (*1c*). Yield (35%). ^{1}H NMR (400 MHz, CDCl₃) δ 7.74 (s, 1H), 5.98 (s, 1H), 5.85 (t, J = 8.0 Hz, 1H), 5.58 (t, J = 9.7 Hz, 1H), 5.19 (s, 1H), 4.21 – 4.16 (m, 1H), 4.07 (d, J = 2.5 Hz, 2H), 4.02 – 3.95 (m, 1H), 3.68 – 3.56 (m, 2H), 3.38 – 3.32 (m, 2H), 2.50 – 2.36 (m, 2H), 2.36 – 2.31 (m, 1H), 2.31 – 2.25 (m, 2H), 2.17 – 2.09 (m, 1H), 2.03 – 1.95 (m, 1H), 1.95 – 1.87 (m, 1H), 1.87 – 1.81 (m, 2H), 1.81 – 1.73 (m, 2H), 1.73 – 1.59 (m, 3H), 1.56 – 1.46 (m, 2H), 1.46 – 1.35 (m, 2H), 0.95 (d, J = 6.5 Hz, 6H).

((1S,3S,5R)-Bicyclo[3.3.1]non-6-en-3-yl)methyl-d2((S)-1-(((S)-1-hydroxy-3-((S)-2-oxopyrrolidin-3-yl)propan-2-yl)amino)-4-methyl-1-oxopentan-2-yl)carbamate (*1d*). Yield (36%). ^{1}H NMR (400 MHz, CDCl₃) δ 7.72 (s, 1H), 6.04 (s, 1H), 5.85 (t, J = 8.1 Hz, 1H), 5.62 – 5.55 (m, 1H), 5.20 (s, 1H), 4.23 – 4.15 (m, 1H), 4.02 – 3.93 (m, 1H), 3.68 – 3.54 (m, 2H), 3.39 – 3.33 (m, 2H), 2.49 – 2.31 (m, 3H), 2.30 – 2.26 (m, 1H), 2.16 – 2.09 (m,

1H), 2.03 – 1.95 (m, 2H), 1.93 – 1.78 (m, 4H), 1.78 – 1.59 (m, 4H), 1.59 – 1.46 (m, 2H), 1.46 – 1.35 (m, 2H), 0.95 (d, *J* = 6.5 Hz, 6H).

Bicyclo[2.2.1]hept-5-en-2-ylmethyl ((S)-1-(((S)-1-hydroxy-3-((S)-2-oxopyrrolidin-3-yl)propan-2-yl)amino)-4-methyl-1-oxopentan-2-yl)carbamate (*1e*). Yield (44%). ^{1}H NMR (400 MHz, CDCl₃) δ 7.74 (s, 1H), 6.38 (s, 1H), 6.14 (dd, *J* = 5.7, 3.0 Hz, 1H), 5.93 (dd, *J* = 5.8, 2.9 Hz, 1H), 5.41 – 5.32 (m, 1H), 4.27 – 4.19 (m, 1H), 4.19 – 4.07 (m, 1H), 4.06 – 3.89 (m, 1H), 3.88 – 3.80 (m, 1H), 3.69 – 3.53 (m, 3H), 3.35 (dd, *J* = 10.6, 4.2 Hz, 2H), 2.87 – 2.77 (m, 2H), 2.52 – 2.34 (m, 2H), 2.10 – 1.87 (m, 1H), 1.87 – 1.77 (m, 1H), 1.77 – 1.57 (m, 3H), 1.57 – 1.47 (m, 1H), 1.47 – 1.40 (m, 1H), 1.37 – 1.18 (m, 1H), 1.18 – 1.10 (m, 1H), 0.96 (d, *J* = 6.5 Hz, 6H), 0.53 (ddd, *J* = 11.7, 4.5, 2.6 Hz, 1H).

Bicyclo[2.2.1]heptan-2-ylmethyl ((S)-1-(((S)-1-hydroxy-3-((S)-2-oxopyrrolidin-3-yl)propan-2-yl)amino)-4-methyl-1-oxopentan-2-yl)carbamate (*1f*). Yield (44%). ^{1}H NMR (400 MHz, CDCl₃) δ 7.73 (s, 1H), 6.30 (s, 1H), 5.30 (s, 1H), 4.30 – 4.15 (m, 1H), 4.15 – 4.04 (m, 1H), 4.04 – 3.95 (m, 1H), 3.95 – 3.85 (m, 1H), 3.78 (d, *J* = 8.0 Hz, 1H), 3.71 – 3.52 (m, 2H), 3.39 – 3.32 (m, 2H), 2.48 – 2.36 (m, 2H), 2.24 – 2.17 (m, 1H), 2.17 – 1.96 (m, 1H), 1.97 – 1.75 (m, 1H), 1.75 – 1.56 (m, 3H), 1.56 – 1.41 (m, 3H), 1.41 – 1.21 (m, 3H), 1.21 – 0.99 (m, 3H), 0.95 (d, *J* = 6.4 Hz, 6H), 0.66 (dd, *J* = 12.6, 5.1 Hz, 1H).

tert-Butyl (1R,3s,5S)-3-(((((S)-1-(((S)-1-hydroxy-3-((S)-2-oxopyrrolidin-3-yl)propan-2-yl)amino)-4-methyl-1-oxopentan-2-yl)carbamoyl)oxy)-8-azabicyclo[3.2.1]octane-8-carboxylate (*1g*). Yield (45%). ^{1}H NMR (400 MHz, CDCl₃) δ 7.85 (s, 1H), 6.29 (s, 1H), 5.31 (d, *J* = 9.3 Hz, 1H), 4.94 (s, 1H), 4.29 – 4.02 (m, 3H), 4.01 – 3.97 (m, 1H), 3.64 – 3.59 (m, 2H), 3.39 – 3.31 (m, 2H), 2.44 – 2.39 (m, 2H), 2.20 – 1.89 (m, 8H), 1.84 (dd, *J* =

11.3, 9.0 Hz, 1H), 1.76 (d, J = 15.2 Hz, 2H), 1.73 – 1.60 (m, 2H), 1.60 – 1.48 (m, 1H), 1.46 (s, 9H), 0.99 – 0.91 (m, 6H).

Benzyl (1R,3s,5S)-3-((((S)-1-(((S)-1-hydroxy-3-((S)-2-oxopyrrolidin-3-yl)propan-2-yl)amino)-4-methyl-1-oxopentan-2-yl)carbamoyl)oxy)-8-azabicyclo[3.2.1]octane-8-carboxylate (*1h*). Yield (49%). ^{1}H NMR (400 MHz, DMSO-d₆) δ 7.60-7.56 (m, 2H), 7.47-7.10 (m, 6H), 5.11 (d, J = 10.53 Hz, 2H), 5.02-4.88 (m, 1H), 4.83-4.61 (m, 1H), 4.30-4.15 (m, 2H), 4.05 (d, J = 7.11 Hz, 1H), 3.97-3.88 (m, 2H), 3.79-3.71 (m, 1H), 3.65-3.56 (m, 2H), 2.79-2.71 (m, 1H), 2.30-1.35 (m, 5H), 1.35 – 0.90 (m, 9H), 0.87 (td, J = 9.48, 8.02, 8.02 Hz, 6H).

(4-Pentylbicyclo[2.2.2]octan-1-yl)methyl ((S)-1-(((S)-1-hydroxy-3-((S)-2-oxopyrrolidin-3-yl)propan-2-yl)amino)-4-methyl-1-oxopentan-2-yl)carbamate (*1i*). Yield (33%). ^{1}H NMR (400 MHz, DMSO-d₆) δ 7.63-7.45 (m, 1H), 7.09-6.97 (m, 2H), 6.94-4.71 (m, 2H), 4.69-4.57 (m, 5H), 2.90 (s, 1H), 2.78-2.70 (m, 1H), 1.95-1.87 (m, 5H), 1.32 (d, J = 7.74 Hz, 6H), 1.23-1.15 (m, 19H), 0.86 (dd, J = 13.86, 6.91 Hz, 6H).

(4-Pentylbicyclo[2.2.2]octan-1-yl)methyl-d2 ((S)-1-(((S)-1-hydroxy-3-((S)-2-oxopyrrolidin-3-yl)propan-2-yl)amino)-4-methyl-1-oxopentan-2-yl)carbamate (*1j*). Yield (20%). ^{1}H NMR (400 MHz, DMSO-d₆) δ 7.62-7.47 (m, 1H), 7.10-6.97 (m, 2H), 6.97-4.75 (m, 2H), 4.69-4.59 (m, 3H), 2.92 (s, 1H), 2.78-2.76 (m, 1H), 1.95-1.87 (m, 5H), 1.39 (d, J = 7.74 Hz, 6H), 1.23-1.17 (m, 19H), 0.86 (dd, J = 13.86, 6.91 Hz, 6H).

((3S,5S,7S)-Adamantan-1-yl)methyl ((S)-1-(((S)-1-hydroxy-3-((S)-2-oxopyrrolidin-3-yl)propan-2-yl)amino)-4-methyl-1-oxopentan-2-yl)carbamate (*1k*). Yield (75%). ^{1}H NMR (400 MHz, CDCl₃) δ 7.75 (d, J = 7.1 Hz, 1H), 6.15 (s, 1H), 5.27 (d, J = 8.1 Hz, 1H), 4.23 – 4.18 (m, 1H), 4.03 – 3.96 (m, 1H), 3.74 – 3.57 (m, 4H), 3.39 – 3.31 (m, 2H), 2.49 – 2.34

(m, 2H), 1.99 – 1.95 (m, 4H), 1.88 – 1.79 (m, 1H), 1.76 – 1.60 (m, 9H), 1.58 – 1.46 (m, 7H), 0.96 (dd, $J = 6.4$, 2.4 Hz, 6H).

((3S,5S,7S)-Adamantan-1-yl)methyl-d2 ((S)-1-(((S)-1-hydroxy-3-((S)-2-oxopyrrolidin-3-yl)propan-2-yl)amino)-4-methyl-1-oxopentan-2-yl)carbamate (**1l**). Yield (26%). ^{1}H NMR (400 MHz, cdcl3) δ 7.73 (d, $J = 7.3$ Hz, 1H), 6.19 (s, 1H), 5.26 (d, $J = 8.1$ Hz, 1H), 4.22 – 4.18 (m, 1H), 4.03 – 3.96 (m, 1H), 3.67 – 3.54 (m, 2H), 3.39 – 3.31 (m, 2H), 2.49 – 2.33 (m, 2H), 2.06 – 2.02 (m, 1H), 1.99 – 1.95 (m, 3H), 1.88 – 1.79 (m, 2H), 1.78 – 1.60 (m, 9H), 1.57 – 1.48 (m, 6H), 0.96 (dd, $J = 6.4$, 2.1 Hz, 6H).

2-((3S,5S,7S)-Adamantan-1-yl)ethyl ((S)-1-(((S)-1-hydroxy-3-((S)-2-oxopyrrolidin-3-yl)propan-2-yl)amino)-4-methyl-1-oxopentan-2-yl)carbamate (**1m**). Yield (65%). ^{1}H NMR (400 MHz, CDCl3) δ 7.73 (d, $J = 7.0$ Hz, 1H), 6.24 (s, 1H), 5.28 (d, $J = 8.3$ Hz, 1H), 4.25 – 4.20 (m, 1H), 4.17 – 4.07 (m, 2H), 4.04 – 3.96 (m, 1H), 3.70 – 3.44 (m, 2H), 3.39 – 3.31 (m, 2H), 2.52 – 2.34 (m, 2H), 2.09 – 1.97 (m, 1H), 1.97 – 1.91 (m, 3H), 1.90 – 1.76 (m, 1H), 1.74 – 1.57 (m, 9H), 1.55 – 1.45 (m, 7H), 1.40 (t, $J = 7.5$ Hz, 2H), 0.95 (d, $J = 6.4$ Hz, 6H).

((1R,3R,5R,7S)-3-Hydroxyadamantan-1-yl)methyl ((S)-1-(((S)-1-hydroxy-3-((S)-2-oxopyrrolidin-3-yl)propan-2-yl)amino)-4-methyl-1-oxopentan-2-yl)carbamate (**1n**). Yield (8%). ^{1}H NMR (400 MHz, CDCl3) δ 7.69 (d, $J = 7.3$ Hz, 1H), 6.34 (s, 1H), 5.45 (d, $J = 8.0$ Hz, 1H), 4.20 – 4.16 (m, 1H), 4.05 – 3.87 (m, 1H), 3.74 – 3.54 (m, 4H), 3.37 – 3.28 (m, 2H), 2.45 – 2.40 (m, 2H), 2.21 (s, 2H), 2.11 – 1.94 (m, 1H), 1.88 – 1.79 (m, 1H), 1.79 – 1.59 (m, 8H), 1.59 – 1.54 (m, 2H), 1.54 – 1.47 (m, 3H), 1.47 – 1.32 (m, 3H), 0.99 – 0.88 (m, 6H).

((1r,3R,5R,7S)-3-Hydroxyadamantan-1-yl)methyl-d2   ((S)-1-(((S)-1-hydroxy-3-((S)-2-oxopyrrolidin-3-yl)propan-2-yl)amino)-4-methyl-1-oxopentan-2-yl)carbamate (**1o**). Yield (7%). ^{1}H NMR (400 MHz, CDCl$_3$) δ 7.70 (d, J = 7.1 Hz, 1H), 6.26 (s, 1H), 5.41 (d, J = 7.9 Hz, 1H), 4.23 – 4.14 (m, 1H), 4.03 – 3.96 (m, 1H), 3.68 – 3.54 (m, 2H), 3.39 – 3.32 (m, 2H), 2.43 (s, 2H), 2.27 – 2.19 (m, 2H), 2.11 – 1.91 (m, 1H), 1.88 – 1.80 (m, 1H), 1.77 – 1.60 (m, 8H), 1.60 – 1.54 (m, 1H), 1.54 – 1.47 (m, 4H), 1.43 – 1.38 (m, 3H), 0.99 – 0.88 (m, 6H).

Preparation of compounds *2(a-o)*. General procedure. To a solution of dipeptidyl alcohol *1* (1 eq) in anhydrous dichloromethane (300 mL/g dipeptidyl alcohol) kept at 0-5 °C under a N$_2$ atmosphere was added Dess-Martin periodinane reagent (3.0 eq) and the reaction mixture was stirred for 3 h at 15-20 °C. The organic phase was washed with 10% aq Na$_2$S$_2$O$_3$ (2 x 100 mL/g dipeptidyl alcohol), followed by saturated aqueous NaHCO$_3$ (2 x 100 mL/ g dipeptidyl alcohol), distilled water (2 x 100 mL/ g dipeptidyl alcohol), and brine (100 mL/ g dipeptidyl alcohol). The organic phase was dried over anhydrous Na$_2$SO$_4$, filtered and concentrated *in vacuo*. The resulting crude product was purified by flash chromatography (hexane/ethyl acetate) to yield aldehyde *2* as a white solid.

((1R,3s,5S)-Bicyclo[3.3.1]nonan-3-yl)methyl   ((S)-4-methyl-1-oxo-1-(((S)-1-oxo-3-((S)-2-oxopyrrolidin-3-yl)propan-2-yl)amino)pentan-2-yl)carbamate (**2a**). Yield (86%). ^{1}H NMR (400 MHz, CDCl$_3$) δ 9.50 (s, 1H), 8.31 (s, 1H), 5.21 (d, J = 8.7 Hz, 1H), 4.38 – 4.28 (m, 2H), 3.96 – 3.87 (m, 2H), 3.40 – 3.31 (m, 2H), 2.54 – 2.36 (m, 2H), 2.08 – 1.99 (m, 3H), 1.99 – 1.81 (m, 5H), 1.76 – 1.63 (m, 6H), 1.60 – 1.49 (m, 1H), 1.46 – 1.29 (m, 4H), 1.15 – 1.05 (m, 1H), 0.97 (d, J = 6.3 Hz, 6H), 0.88 (d, J = 13.4 Hz, 2H). HRMS m/z: [M+H]$^+$

Calculated for $C_{24}H_{40}N_3O_5$: 450.2968, Found: 450.2958, m/z: [M+Na]+ Calculated for $C_{24}H_{39}N_3NaO_5$: 472.2788, Found: 472.2776.

((1R,3s,5S)-Bicyclo[3.3.1]nonan-3-yl)methyl-d2 ((S)-4-methyl-1-oxo-1-(((S)-1-oxo-3-((S)-2-oxopyrrolidin-3-yl)propan-2-yl)amino)pentan-2-yl)carbamate (**2b**). Yield (85%). ^{1}H NMR (400 MHz, CDCl$_3$) δ 9.50 (s, 1H), 8.30 (s, 1H), 6.16 (s, 1H), 5.24 (d, *J* = 8.6 Hz, 1H), 4.38 − 4.29 (m, 2H), 3.41 − 3.30 (m, 2H), 2.52 − 2.34 (m, 2H), 2.12 − 1.99 (m, 3H), 1.98 − 1.78 (m, 4H), 1.78 − 1.62 (m, 4H), 1.61 − 1.51 (m, 1H), 1.41 − 1.30 (m, 6H), 1.13 − 1.06 (m, 1H), 0.97 (d, *J* = 6.3 Hz, 6H), 0.96 − 0.83 (m, 2H). HRMS m/z: [M+Na]+ Calculated for $C_{24}H_{37}D_2N_3NaO_5$: 474.2913, Found: 474.2897.

((1S,5R)-Bicyclo[3.3.1]non-6-en-3-yl)methyl ((S)-4-methyl-1-oxo-1-(((S)-1-oxo-3-((S)-2-oxopyrrolidin-3-yl)propan-2-yl)amino)pentan-2-yl)carbamate (**2c**). Yield (53%). ^{1}H NMR (400 MHz, CDCl$_3$) δ 9.49 (s, 1H), 8.27 (s, 1H), 6.04 (s, 1H), 5.86 (t, *J* = 7.1 Hz, 1H), 5.63 − 5.55 (m, 1H), 5.18 (d, *J* = 8.5 Hz, 1H), 4.38 − 4.27 (m, 2H), 4.10 − 4.03 (m, 1H), 4.03 − 3.94 (m, 1H), 3.41 − 3.31 (m, 2H), 2.52 − 2.37 (m, 1H), 2.28 (s, 2H), 2.18 − 2.08 (m, 1H), 2.01 − 1.92 (m, 3H), 1.92 − 1.83 (m, 3H), 1.83 − 1.71 (m, 1H), 1.71 − 1.66 (m, 4H), 1.62 − 1.49 (m, 3H), 1.49 − 1.36 (m, 1H), 0.97 (d, *J* = 6.4 Hz, 6H). HRMS m/z: [M+H]+ Calculated for $C_{24}H_{38}N_3O_5$: 448.2811, Found: 448.2810, m/z: [M+Na]+ Calculated for $C_{24}H_{37}N_3NaO_5$: 470.2631, Found: 470.2628.

((1S,3S,5R)-Bicyclo[3.3.1]non-6-en-3-yl)methyl-d2 ((S)-4-methyl-1-oxo-1-(((S)-1-oxo-3-((S)-2-oxopyrrolidin-3-yl)propan-2-yl)amino)pentan-2-yl)carbamate (**2d**). Yield (88%). ^{1}H NMR (400 MHz, CDCl$_3$) δ 9.49 (s, 1H), 8.28 (d, *J* = 6.1 Hz, 1H), 6.33 (s, 1H), 5.85 (t, *J* = 8.0 Hz, 1H), 5.58 (d, *J* = 9.9 Hz, 1H), 5.24 (d, *J* = 8.7 Hz, 1H), 4.38 − 4.29 (m, 2H), 3.43 − 3.30 (m, 2H), 2.54 − 2.32 (m, 2H), 2.31 − 2.26 (m, 1H), 2.20 − 2.08 (m, 1H), 2.08 − 1.62

(m, 9H), 1.62 – 1.46 (m, 4H), 1.45 – 1.38 (m, 2H), 0.97 (d, J = 6.1 Hz, 6H). HRMS m/z: [M+Na]$^+$ Calculated for $C_{24}H_{35}D_2N_3NaO_5$: 472.2757, Found: 472.2743.

Bicyclo[2.2.1]hept-5-en-2-ylmethyl ((S)-4-methyl-1-oxo-1-(((S)-1-oxo-3-((S)-2-oxopyrrolidin-3-yl)propan-2-yl)amino)pentan-2-yl)carbamate (**2e**). Yield (84%). ^{1}H NMR (400 MHz, CDCl$_3$) δ 9.50 (s, 1H), 8.30 (d, J = 6.7 Hz, 1H), 6.39 (s, 1H), 6.14 (dd, J = 5.8, 3.1 Hz, 1H), 5.93 (dd, J = 5.7, 2.9 Hz, 1H), 5.27 (s, 1H), 4.38 – 4.31 (m, 2H), 3.89 – 3.80 (m, 1H), 3.69 – 3.60 (m, 1H), 3.43 – 3.30 (m, 2H), 2.89 – 2.78 (m, 1H), 2.56 – 2.31 (m, 3H), 2.11 – 1.96 (m, 1H), 1.96 – 1.90 (m, 1H), 1.90 – 1.78 (m, 2H), 1.78 – 1.63 (m, 2H), 1.63 – 1.49 (m, 1H), 1.48 – 1.33 (m, 1H), 1.29 – 1.18 (m, 1H), 1.19 – 1.10 (m, 1H), 0.97 (d, J = 6.3 Hz, 6H), 0.58 – 0.50 (m, 1H). HRMS m/z: [M+Na]$^+$ Calculated for $C_{22}H_{33}N_3NaO_5$: 442.2318, Found: 442.2310.

Bicyclo[2.2.1]heptan-2-ylmethyl ((S)-4-methyl-1-oxo-1-(((S)-1-oxo-3-((S)-2-oxopyrrolidin-3-yl)propan-2-yl)amino)pentan-2-yl)carbamate (**2f**). Yield (88%). ^{1}H NMR (400 MHz, CDCl$_3$) δ 9.50 (s, 1H), 8.29 (s, 1H), 6.34 (s, 1H), 5.26 (s, 1H), 4.39 – 4.29 (m, 2H), 4.14 – 4.03 (m, 1H), 3.97 – 3.86 (m, 1H), 3.84 – 3.72 (m, 1H), 3.43 – 3.30 (m, 2H), 2.54 – 2.34 (m, 2H), 2.29 – 2.15 (m, 2H), 2.16 – 2.08 (m, 1H), 2.08 – 1.77 (m, 1H), 1.77 – 1.63 (m, 3H), 1.59 – 1.43 (m, 2H), 1.41 – 1.23 (m, 4H), 1.22 – 1.02 (m, 2H), 0.97 (d, J = 6.3 Hz, 6H), 0.67 (ddd, J = 12.5, 5.4, 2.3 Hz, 1H). HRMS m/z: [M+Na]$^+$ Calculated for $C_{22}H_{35}N_3NaO_5$: 444.2475, Found: 444.2467.

tert-Butyl (1R,3s,5S)-3-((((S)-4-methyl-1-oxo-1-(((S)-1-oxo-3-((S)-2-oxopyrrolidin-3-yl)propan-2-yl)amino)pentan-2-yl)carbamoyl)oxy)-8-azabicyclo[3.2.1]octane-8-carboxylate (**2g**). Yield (90%). ^{1}H NMR (400 MHz, CDCl$_3$) δ 9.49 (s, 1H), 8.43 (d, J = 5.6 Hz, 1H), 6.07 (s, 1H), 5.20 (d, J = 8.6 Hz, 1H), 4.96 (s, 1H), 4.35 – 4.28 (m, 2H), 4.25 –

4.09 (m, 2H), 3.41 – 3.33 (m, 2H), 2.53 – 2.36 (m, 2H), 2.23 – 1.94 (m, 8H), 1.94 – 1.82 (m, 1H), 1.81 – 1.64 (m, 4H), 1.61 – 1.52 (m, 1H), 1.46 (s, 9H), 0.98 (d, J = 5.0 Hz, 6H). HRMS m/z: [M+H]$^+$ Calculated for $C_{26}H_{43}N_4O_7$: 523.3131, Found: 523.3116. HRMS m/z: [M+Na]$^+$ Calculated for $C_{26}H_{42}N_4NaO_7$: 545.2951, Found: 545.2938.

Benzyl (1R,3s,5S)-3-((((S)-4-methyl-1-oxo-1-(((S)-1-oxo-3-((S)-2-oxopyrrolidin-3-yl)propan-2-yl)amino)pentan-2-yl)carbamoyl)oxy)-8-azabicyclo[3.2.1]octane-8-carboxylate (**2h**). Yield (66%). ^{1}H NMR (400 MHz, DMSO-d_6) δ 9.39 (s, 1H), 8.55-8.35 (m, 1H), 8.11-8.02 (m, 1H), 7.64 (s, 1H), 7.45-7.19 (m, 5H), 5.75 (s, 1H), 5.09 (d, J = 10.47 Hz, 2H), 4.83-4.71 (m, 2H), 4.21 (s, 2H), 3.73-3.57 (m, 2H), 3.24-3.00 (m, 2H), 2.34-1.79 (m, 3H), 1.79-1.34 (m, 2H), 1.28-1.12 (m, 9H), 0.98-0.77 (m, 6H). HRMS m/z: [M+H]$^+$ Calculated for $C_{29}H_{41}N_4O_7$: 557.2970, Found: 557.2962. HRMS m/z: [M+Na]$^+$ Calculated for $C_{29}H_{40}N_4NaO_7$: 579.2789, Found: 579.2773.

(4-Pentylbicyclo[2.2.2]octan-1-yl)methyl ((S)-4-methyl-1-oxo-1-(((S)-1-oxo-3-((S)-2-oxopyrrolidin-3-yl)propan-2-yl)amino)pentan-2-yl)carbamate (**2i**). Yield (59%). ^{1}H NMR (400 MHz, DMSO-d_6) δ 9.49 (s, 1H), 7.66-7.58 (m, 1H), 7.54-7.44 (m, 2H), 5.72-5.64 (m, 2H), 3.71-3.53 (m, 5H), 3.21-3.13 (m, 1H), 2.93-2.85 (m, 1H), 2.77-2.69 (m, 1H), 2.30-2.22 (m, 1H), 1.91 (s, 1H), 1.63-1.55 (m, 5H), 1.42-0.96 (m, 20H), 0.87 (td, J = 19.27, 6.96, 6.96 Hz, 6H). HRMS m/z: [M+Na]$^+$ Calculated for $C_{28}H_{47}N_3NaO_5$: 528.3414, Found: 528.3391.

(4-Pentylbicyclo[2.2.2]octan-1-yl)methyl-d2 ((S)-4-methyl-1-oxo-1-(((S)-1-oxo-3-((S)-2-oxopyrrolidin-3-yl)propan-2-yl)amino)pentan-2-yl)carbamate (**2j**). Yield (49%). ^{1}H NMR (400 MHz, DMSO-d_6) δ 9.49 (s, 1H), 7.66-7.58 (m, 1H), 7.54-7.44 (m, 2H), 5.72-5.64 (m, 2H), 3.71-3.63 (m, 3H), 3.31 (s, 1H), 2.93-2.85 (m, 1H), 2.85-2.69 (m, 1H), 2.30-2.22 (m,

1H), 1.91 (s, 1H), 1.42-0.96 (m, 25H), 0.87 (td, J = 19.21, 6.96, 6.96 Hz, 6H). HRMS m/z: [M+Na]$^+$ Calculated for $C_{28}H_{45}D_2N_3NaO_5$: 530.3539, Found: 530.3536.

((3S,5S,7S)-Adamantan-1-yl)methyl((S)-4-methyl-1-oxo-1-(((S)-1-oxo-3-((S)-2-oxopyrrolidin-3-yl)propan-2-yl)amino)pentan-2-yl)carbamate (**2k**). Yield (90%). ^{1}H NMR (400 MHz, CDCl$_3$) δ 9.50 (s, 1H), 8.31 (d, J = 5.8 Hz, 1H), 6.36 (s, 1H), 5.27 (s, 1H), 4.39 − 4.29 (m, 2H), 3.66 (s, 2H), 3.41 − 3.30 (m, 2H), 2.55 − 2.34 (m, 2H), 2.08 − 1.92 (m, 3H), 1.92 − 1.78 (m, 2H), 1.78 − 1.60 (m, 9H), 1.52 (d, J = 2.9 Hz, 7H), 1.00 − 0.94 (m, 6H). HRMS m/z: [M+Na]$^+$ Calculated for $C_{25}H_{39}N_3NaO_5$: 484.2788, Found: 484.2780.

((3S,5S,7S)-Adamantan-1-yl)methyl-d2 ((S)-4-methyl-1-oxo-1-(((S)-1-oxo-3-((S)-2-oxopyrrolidin-3-yl)propan-2-yl)amino)pentan-2-yl)carbamate (**2l**). Yield (88%). ^{1}H NMR (400 MHz, cdcl$_3$) δ 9.49 (s, 1H), 8.32 (d, J = 5.9 Hz, 1H), 6.13 (d, J = 8.1 Hz, 1H), 5.23 (s, 1H), 4.68 − 4.58 (m, 1H), 4.38 − 4.25 (m, 1H), 3.41 − 3.27 (m, 2H), 2.52 − 2.34 (m, 2H), 2.06 − 2.01 (m, 2H), 2.00 − 1.89 (m, 3H), 1.88 − 1.78 (m, 4H), 1.78 − 1.55 (m, 9H), 1.52 (d, J = 2.9 Hz, 3H), 1.00 − 0.91 (m, 6H). HRMS m/z: [M+Na]$^+$ Calculated for $C_{25}H_{37}D_2N_3NaO_5$: 486.2913, Found: 486.2910.

2-((3S,5S,7S)-Adamantan-1-yl)ethyl ((S)-4-methyl-1-oxo-1-(((S)-1-oxo-3-((S)-2-oxopyrrolidin-3-yl)propan-2-yl)amino)pentan-2-yl)carbamate (**2m**). Yield (83%). ^{1}H NMR (400 MHz, CDCl$_3$) δ 9.50 (s, 1H), 8.30 (d, J = 5.9 Hz, 1H), 6.09 (d, J = 11.7 Hz, 1H), 5.19 (d, J = 8.7 Hz, 1H), 4.38 − 4.28 (m, 2H), 4.26 − 4.05 (m, 2H), 3.41 − 3.33 (m, 2H), 2.54 − 2.35 (m, 2H), 2.01 − 1.91 (m, 4H), 1.91 − 1.79 (m, 1H), 1.74 − 1.58 (m, 9H), 1.51 (d, J = 2.9 Hz, 6H), 1.41 (t, J = 7.4 Hz, 2H), 1.28 − 1.23 (m, 1H), 0.97 (d, J = 6.4 Hz, 6H). HRMS m/z: [M+H]$^+$ Calculated for $C_{26}H_{42}N_3O_5$: 476.3124, Found: 476.3124. HRMS m/z: [M+Na]$^+$ Calculated for $C_{26}H_{41}N_3NaO_5$: 498.2944, Found: 498.2938.

((1r,3R,5R,7S)-3-Hydroxyadamantan-1-yl)methyl ((S)-4-methyl-1-oxo-1-(((S)-1-oxo-3-((S)-2-oxopyrrolidin-3-yl)propan-2-yl)amino)pentan-2-yl)carbamate (**2n**). Yield (47%). ^{1}H NMR (400 MHz, CDCl$_3$) δ 9.49 (s, 1H), 8.28 (d, J = 23.9 Hz, 1H), 6.19 (s, 1H), 5.19 (s, 1H), 4.34 – 4.03 (m, 2H), 4.02 – 3.61 (m, 2H), 2.89 – 2.58 (m, 2H), 2.58 – 2.28 (m, 2H), 2.28 – 2.13 (m, 3H), 2.09 – 1.76 (m, 2H), 1.78 – 1.60 (m, 6H), 1.57 – 1.31 (m, 9H), 1.01 – 0.91 (m, 6H). HRMS m/z: [M+Na]$^+$ Calculated for C$_{25}$H$_{39}$N$_3$NaO$_6$: 500.2737, Found: 500.2739.

((1r,3R,5R,7S)-3-Hydroxyadamantan-1-yl)methyl-d2 ((S)-4-methyl-1-oxo-1-(((S)-1-oxo-3-((S)-2-oxopyrrolidin-3-yl)propan-2-yl)amino)pentan-2-yl)carbamate (**2o**). Yield (44%). ^{1}H NMR (400 MHz, CDCl$_3$) δ 9.48 (s, 1H), 8.28 (d, J = 6.5 Hz, 1H), 6.39 (s, 1H), 5.12 (s, 1H), 4.40 – 4.09 (m, 2H), 2.89 – 2.59 (m, 2H), 2.56 – 2.30 (m, 2H), 2.30 – 2.20 (m, 3H), 2.18 – 1.77 (m, 2H), 1.77 – 1.61 (m, 6H), 1.59 – 1.39 (m, 9H), 1.01 – 0.89 (m, 6H). HRMS m/z: [M+Na]$^+$ Calculated for C$_{25}$H$_{37}$D$_2$N$_3$NaO$_6$: 502.2862, Found: 502.2860.

Preparation of compounds *3(a-o)*. General procedure. To a solution of dipeptidyl aldehyde **2** (1 eq) in ethyl acetate (10 mL/g of dipeptidyl aldehyde) was added absolute ethanol (5 mL/g of dipeptidyl aldehyde) with stirring, followed by a solution of sodium bisulfite (1 eq) in water (1 mL/ g of dipeptidyl aldehyde). The reaction mixture was stirred for 3 h at 50 °C. The reaction mixture was allowed to cool to room temperature and then vacuum filtered. The solid was thoroughly washed with absolute ethanol and the filtrate was dried over anhydrous sodium sulfate, filtered, and concentrated to yield a white solid. The white solid was stirred with dry ethyl ether (3 x 10 mL/ g of dipeptidyl aldehyde), followed by careful removal of the solvent using a pipette and dried using a vacuum pump for 2 h to yield dipeptidyl bisulfite adduct **3** as a white solid.

Sodium (2S)-2-((2S)-2-(((((1R,5S)-bicyclo[3.3.1]nonan-3-yl)methoxy)carbonyl)amino)-4-methylpentanamido)-1-hydroxy-3-((S)-2-oxopyrrolidin-3-yl)propane-1-sulfonate (**3a**). Yield (66%). ^{1}H NMR (400 MHz, DMSO-d$_6$) δ 7.61 (d, J = 9.0 Hz, 1H), 7.57 − 7.44 (m, 1H), 7.28 − 7.08 (m, 1H), 5.62 (d, J = 6.1 Hz, 1H), 5.47 (d, J = 5.9 Hz, 1H), 4.12 − 3.91 (m, 2H), 3.91 − 3.73 (m, 2H), 3.16 − 3.00 (m, 2H), 2.24 − 2.07 (m, 2H), 2.06 − 1.95 (m, 2H), 1.83 (dt, J = 17.2, 7.2 Hz, 4H), 1.74 − 1.51 (m, 5H), 1.51 − 1.38 (m, 2H), 1.35 − 1.15 (m, 6H), 1.14 − 1.00 (m, 2H), 0.99 − 0.81 (m, 6H). HRMS m/z: [M+Na]$^+$ Calculated for C$_{24}$H$_{40}$N$_3$Na$_2$O$_8$S: 576.2332, Found: 576.2329, m/z: [M]$^-$ Calculated for C$_{24}$H$_{40}$N$_3$O$_8$S: 530.2536, Found: 530.2529.

Sodium (2S)-2-((S)-2-(((((1R,3s,5S)-bicyclo[3.3.1]nonan-3-yl)methoxy-d2)carbonyl)amino)-4-methylpentanamido)-1-hydroxy-3-((S)-2-oxopyrrolidin-3-yl)propane-1-sulfonate (**3b**). Yield (75%). ^{1}H NMR (400 MHz, DMSO-d$_6$) δ 7.63 − 7.43 (m, 2H), 7.20 (dd, J = 20.3, 8.2 Hz, 1H), 5.52 − 5.33 (m, 1H), 4.06 − 3.78 (m, 2H), 3.20 − 2.99 (m, 2H), 2.33 − 2.04 (m, 3H), 2.04 − 1.93 (m, 2H), 1.94 − 1.74 (m, 2H), 1.74 − 1.50 (m, 3H), 1.50 − 1.38 (m, 2H), 1.38 − 1.19 (m, 5H), 1.11 − 0.98 (m, 2H), 0.97 − 0.80 (m, 10H). HRMS m/z: [M+Na]$^+$ Calculated for C$_{24}$H$_{38}$D$_2$N$_3$Na$_2$O$_8$S: 578.2457, Found: 578.2432.

Sodium (2S)-2-((2S)-2-(((((1S,5R)-bicyclo[3.3.1]non-6-en-3-yl)methoxy)carbonyl)amino)-4-methylpentanamido)-1-hydroxy-3-((S)-2-oxopyrrolidin-3-yl)propane-1-sulfonate (**3c**). Yield (66%). ^{1}H NMR (400 MHz, DMSO-d$_6$) δ 7.52 (d, J = 9.5 Hz, 1H), 7.47 (d, J = 4.5 Hz, 1H), 7.18 (ddd, J = 19.5, 8.5, 2.7 Hz, 1H), 5.89 − 5.79 (m, 1H), 5.58 − 5.52 (m, 1H), 3.97 (h, J = 8.1 Hz, 1H), 3.90 − 3.70 (m, 1H), 3.27 − 3.00 (m, 2H), 2.35 − 2.19 (m, 3H), 2.19 − 2.02 (m, 3H), 2.02 − 1.68 (m, 6H), 1.68 − 1.49 (m, 4H), 1.49 − 1.25 (m, 6H), 1.13

– 1.04 (m, 1H), 0.91 – 0.79 (m, 6H). HRMS m/z: [M+Na]$^+$ Calculated for $C_{24}H_{38}N_3Na_2O_8S$: 574.2175, Found: 574.2163, m/z: [M]$^-$ Calculated for $C_{24}H_{38}N_3O_8S$: 528.2379, Found: 528.2367.

Sodium (2S)-2-((S)-2-(((((1S,3S,5R)-bicyclo[3.3.1]non-6-en-3-yl)methoxy-d2)carbonyl)amino)-4-methylpentanamido)-1-hydroxy-3-((S)-2-oxopyrrolidin-3-yl)propane-1-sulfonate (**3d**). Yield (53%). ^{1}H NMR (400 MHz, DMSO-d$_6$) δ 7.62 – 7.39 (m, 2H), 7.18 (dd, *J* = 24.9, 8.5 Hz, 1H), 5.89 – 5.80 (m, 1H), 5.59 – 5.52 (m, 1H), 5.43 – 5.26 (m, 1H), 4.06 – 3.67 (m, 2H), 3.22 – 2.98 (m, 2H), 2.37 – 2.03 (m, 5H), 2.03 – 1.64 (m, 5H), 1.64 – 1.52 (m, 3H), 1.52 – 1.29 (m, 5H), 1.13 – 1.02 (m, 1H), 0.89 – 0.80 (m, 6H). HRMS m/z: [M+Na]$^+$ Calculated for $C_{24}H_{36}D_2N_3Na_2O_8S$: 576.2301, Found: 576.2275.

Sodium (2S)-2-((2S)-2-(((bicyclo[2.2.1]hept-5-en-2-ylmethoxy)carbonyl)amino)-4-methylpentanamido)-1-hydroxy-3-((S)-2-oxopyrrolidin-3-yl)propane-1-sulfonate (**3e**). Yield (56%). ^{1}H NMR (400 MHz, DMSO-d$_6$) δ 7.68 – 7.37 (m, 2H), 7.32 – 7.17 (m, 1H), 6.20 – 6.02 (m, 1H), 6.02 – 5.86 (m, 1H), 5.59 – 5.30 (m, 1H), 4.11 – 3.79 (m, 2H), 3.79 – 3.41 (m, 2H), 3.21 – 2.98 (m, 2H), 2.87 – 2.66 (m, 2H), 2.39 – 2.04 (m, 3H), 2.04 – 1.85 (m, 1H), 1.85 – 1.70 (m, 1H), 1.70 – 1.51 (m, 2H), 1.50 – 1.36 (m, 2H), 1.28 (dd, *J* = 39.4, 7.9 Hz, 2H), 1.18 – 1.00 (m, 1H), 0.93 – 0.79 (m, 6H), 0.47 (d, *J* = 11.6 Hz, 1H). HRMS m/z: [M+Na]$^+$ Calculated for $C_{22}H_{34}N_3Na_2O_8S$: 546.1862, Found: 546.1842.

Sodium (2S)-2-((2S)-2-(((bicyclo[2.2.1]heptan-2-ylmethoxy)carbonyl)amino)-4-methylpentanamido)-1-hydroxy-3-((S)-2-oxopyrrolidin-3-yl)propane-1-sulfonate (**3f**). Yield (66%). ^{1}H NMR (400 MHz, DMSO-d$_6$) δ 7.61 – 7.39 (m, 2H), 7.32 – 7.08 (m, 1H), 5.41 (dd, *J* = 55.1, 5.9 Hz, 1H), 4.07 – 3.55 (m, 2H), 3.18 – 2.99 (m, 2H), 2.28 – 2.04 (m, 6H), 2.04 – 1.81 (m, 1H), 1.81 – 1.53 (m, 3H), 1.53 – 1.36 (m, 5H), 1.36 – 1.18 (m, 3H),

1.18 – 0.91 (m, 2H), 0.90 – 0.75 (m, 6H), 0.70 – 0.59 (m, 1H). HRMS m/z: [M+Na]$^+$

Calculated for $C_{22}H_{36}N_3Na_2O_8S$: 548.2019, Found: 548.1999.

Sodium (2S)-2-((S)-2-(((((1R,3s,5S)-8-(tert-butoxycarbonyl)-8-azabicyclo[3.2.1]octan-3-yl)oxy)carbonyl)amino)-4-methylpentanamido)-1-hydroxy-3-((S)-2-oxopyrrolidin-3-yl)propane-1-sulfonate (3g). Yield (52%). ^{1}H NMR (400 MHz, DMSO-d$_6$) δ 7.64 – 7.51 (m, 1H), 7.46 (d, *J* = 3.8 Hz, 1H), 7.30 (dd, *J* = 19.2, 8.3 Hz, 1H), 5.55 – 5.31 (m, 1H), 4.76 (s, 1H), 4.02 – 3.78 (m, 4H), 3.22 – 2.98 (m, 2H), 2.27 – 1.68 (m, 9H), 1.66 – 1.57 (m, 4H), 1.51 – 1.43 (m, 2H), 1.40 (s, 9H), 1.13 – 1.02 (m, 1H), 0.91 – 0.81 (m, 6H). HRMS m/z: [M+Na]$^+$ Calculated for $C_{26}H_{43}N_4Na_2O_{10}S$: 649.2496, Found: 649.2500.

Sodium (2S)-2-((S)-2-(((((1R,3s,5S)-8-((benzyloxy)carbonyl)-8-azabicyclo[3.2.1]octan-3-yl)oxy)carbonyl)amino)-4-methylpentanamido)-1-hydroxy-3-((S)-2-oxopyrrolidin-3-yl)propane-1-sulfonate (3h). Yield (53%). 1H NMR (400 MHz, DMSO-d$_6$) δ 7.37 (t, *J* = 4.74, 4.74 Hz, 8H), 5.09 (d, *J* = 11.06 Hz, 2H), 4.29-4.13 (m, 5H), 3.96-3.82 (m, 1H), 3.79-3.69 (m, 1H), 3.17-3.09 (m, 1H), 3.06-2.98 (m, 1H), 2.05-1.81 (m, 5H), 1.74-1.63 (m, 3H), 1.58-1.49 (m, 4H), 1.47-1.33 (m, 2H), 1.08 (dd, *J* = 13.72, 6.78 Hz, 1H), 0.84 (ddd, *J* = 10.35, 8.11, 4.59 Hz, 6H). HRMS m/z: [M+Na]$^+$ Calculated for $C_{29}H_{41}N_4Na_2O_{10}S$: 683.2339, Found: 683.2317.

Sodium (2S)-1-hydroxy-2-((S)-4-methyl-2-((((4-pentylbicyclo[2.2.2]octan-1-yl)methoxy)carbonyl)amino)pentanamido)-3-((S)-2-oxopyrrolidin-3-yl)propane-1-sulfonate (3i). Yield (57%). 1H NMR (400 MHz, DMSO-d$_6$) δ 7.51-7.40 (m, 3H), 4.00 – 3.53 (m, 5H), 3.49-3.40 (m, 1H), 3.16-2.98 (m, 4H), 1.94-1.85 (m, 3H), 1.65-0.96 (m, 25H), 0.85 (dd, *J* = 12.73, 5.76 Hz, 6H). HRMS m/z: [M+Na]$^+$ Calculated for

$C_{28}H_{48}N_3Na_2O_8S$: 632.2958, Found: 632.2932. HRMS m/z: [M]$^-$ Calculated for $C_{28}H_{48}N_3O_8S$: 586.3168, Found: 586.3163.

Sodium (2S)-1-hydroxy-2-((S)-4-methyl-2-((((4-pentylbicyclo[2.2.2]octan-1-yl)methoxy-d2)carbonyl)amino)pentanamido)-3-((S)-2-oxopyrrolidin-3-yl)propane-1-sulfonate (**3j**). Yield (50%). 1H NMR (400 MHz, DMSO-d$_6$) δ 7.51-7.40 (m, 3H), 4.00 – 3.53 (m, 3H), 3.40-3.26 (m, 1H), 3.16-2.90 (m, 3H), 2.56-2.44 (m, 1H), 1.95-1.85 (m, 3H), 1.65-0.96 (m, 25H), 0.85 (dd, *J* = 12.73, 5.76 Hz, 6H). HRMS m/z: [M+Na]$^+$ Calculated for $C_{28}H_{46}D_2N_3Na_2O_8S$: 634.3083, Found: 634.3071. HRMS m/z: [M]$^-$ Calculated for $C_{28}H_{46}D_2N_3O_8S$: 588.3287, Found: 588.3399.

Sodium (2S)-2-((S)-2-((((((3S,5S,7S)-adamantan-1-yl)methoxy)carbonyl)amino)-4-methylpentanamido)-1-hydroxy-3-((S)-2-oxopyrrolidin-3-yl)propane-1-sulfonate (**3k**). Yield (52%). ^{1}H NMR (400 MHz, DMSO-d$_6$) δ 7.66 – 7.41 (m, 2H), 7.25 – 7.10 (m, 1H), 5.40 (dd, *J* = 47.1, 6.0 Hz, 1H), 4.10 – 3.70 (m, 2H), 3.69 – 3.47 (m, 2H), 3.18 – 3.00 (m, 2H), 2.24 – 2.03 (m, 2H), 2.03 – 1.83 (m, 4H), 1.83 – 1.55 (m, 8H), 1.55 – 1.33 (m, 6H), 1.13 – 1.02 (m, 1H), 0.93 – 0.80 (m, 6H). HRMS m/z: [M+Na]$^+$ Calculated for $C_{25}H_{40}N_3Na_2O_8S$: 588.2332, Found: 588.2310.

sodium (2S)-2-((S)-2-(((((3S,5S,7S)-adamantan-1-yl)methoxy-d2)carbonyl)amino)-4-methylpentanamido)-1-hydroxy-3-((S)-2-oxopyrrolidin-3-yl)propane-1-sulfonate (**3l**). Yield (39%). ^{1}H NMR (400 MHz, DMSO-d$_6$) δ 7.63 – 7.50 (m, 1H), 7.47 – 7.36 (m, 1H), 7.38 – 7.28 (m, 1H), 5.41 (dd, *J* = 36.5, 6.0 Hz, 1H), 4.27 – 4.19 (m, 1H), 3.99 – 3.94 (m, 1H), 3.49 – 3.34 (m, 1H), 3.21 – 3.01 (m, 2H), 2.25 – 1.99 (m, 2H), 1.99 – 1.90 (m, 3H), 1.89 – 1.73 (m, 3H), 1.72 – 1.52 (m, 9H), 1.48 (s, 5H), 0.90 – 0.76 (m, 6H). HRMS m/z: [M+Na]$^+$ Calculated for $C_{25}H_{38}D_2N_3Na_2O_8S$: 590.2457, Found: 590.2447.

Sodium (2S)-2-((S)-2-(((2-((3S,5S,7S)-adamantan-1-yl)ethoxy)carbonyl)amino)-4-methylpentanamido)-1-hydroxy-3-((S)-2-oxopyrrolidin-3-yl)propane-1-sulfonate (**3m**). Yield (60%). ^{1}H NMR (400 MHz, DMSO-d_6) δ 7.62 – 7.49 (m, 1H), 7.49 – 7.43 (m, 1H), 7.24 – 7.07 (m, 1H), 5.40 (dd, *J* = 48.6, 6.1 Hz, 1H), 4.05 – 3.81 (m, 4H), 3.20 – 3.00 (m, 2H), 2.26 – 2.06 (m, 2H), 2.01 – 1.87 (m, 3H), 1.84 – 1.72 (m, 1H), 1.70 – 1.54 (m, 10H), 1.49 (d, *J* = 3.0 Hz, 6H), 1.45 – 1.38 (m, 1H), 1.38 – 1.28 (m, 2H), 0.89 – 0.80 (m, 6H). HRMS m/z: [M+Na]$^+$ Calculated for $C_{26}H_{42}N_3Na_2O_8S$: 602.2488, Found: 602.2480.

Sodium (2S)-1-hydroxy-2-((S)-2-(((((1r,3R,5R,7S)-3-hydroxyadamantan-1-yl)methoxy)carbonyl)amino)-4-methylpentanamido)-3-((S)-2-oxopyrrolidin-3-yl)propane-1-sulfonate (**3n**). Yield (69%). ^{1}H NMR (400 MHz, acetone) δ 7.08 – 7.03 (m, 1H), 7.00 – 6.95 (m, 1H), 6.45 – 6.41 (m, 1H), 4.38 – 3.89 (m, 2H), 3.89 – 3.53 (m, 2H), 2.96 – 2.53 (m, 1H), 2.53 – 2.25 (m, 2H), 2.16 (s, 2H), 1.99 – 1.70 (m, 4H), 1.70 – 1.62 (m, 5H), 1.62 – 1.53 (m, 4H), 1.53 – 1.35 (m, 5H), 1.34 – 1.16 (m, 1H), 0.99 – 0.85 (m, 6H). HRMS m/z: [M+Na]$^+$ Calculated for $C_{25}H_{40}N_3Na_2O_9S$: 604.2282, Found: 604.2273.

Sodium (2S)-1-hydroxy-2-((S)-2-(((((1r,3R,5R,7S)-3-hydroxyadamantan-1-yl)methoxy-d2)carbonyl)amino)-4-methylpentanamido)-3-((S)-2-oxopyrrolidin-3-yl)propane-1-sulfonate (**3o**). Yield (73%). ^{1}H NMR (400 MHz, acetone) δ 7.10 – 7.05 (m, 1H), 6.91 – 6.87 (m, 1H), 6.43 – 6.38 (m, 1H), 4.33 – 4.06 (m, 2H), 3.33 – 3.19 (m, 2H), 2.50 – 2.24 (m, 1H), 2.22 – 2.10 (m, 3H), 2.03 – 1.71 (m, 2H), 1.70 – 1.61 (m, 5H), 1.61 – 1.52 (m, 5H), 1.52 – 1.38 (m, 6H), 1.01 – 0.85 (m, 6H). HRMS m/z: [M+Na]$^+$ Calculated for $C_{25}H_{38}D_2N_3Na_2O_9S$: 606.2406, Found: 606.2409.

Biochemical Studies

Enzyme assays and inhibition studies. *Cloning and expression of the 3CL protease of SARS-CoV-2 and FRET enzyme assays.* The codon-optimized cDNA of full length of 3CLpro of SARS-CoV-2 (GenBank number MN908947.3) fused with sequences encoding 6 histidine at the N-terminal was synthesized by Integrated DNA (Coralville, IA). The synthesized gene was subcloned into the pET-28a(+) vector. The expression and purification of SARS-CoV-2 3CLpro were conducted following a standard procedure described previously.[17-18,25] Briefly, a stock solution of an inhibitor was prepared in DMSO and diluted in assay buffer comprised of 20 mM HEPES buffer, pH 8, containing NaCl (200 mM), EDTA (0.4 mM), glycerol (60%), and 6 mM dithiothreitol (DTT). The SARS-CoV-2 protease was mixed with serial dilutions of inhibitor or with DMSO in 25 µL of assay buffer and incubated at 37°C for 1 h, followed by the addition of 25 µL of assay buffer containing substrate (FAM-SAVLQ/SG-QXL®520, AnaSpec, Fremont, CA). The substrate was derived from the cleavage sites on the viral polyproteins of SARS-CoV. Fluorescence readings were obtained using an excitation wavelength of 480 nm and an emission wavelength of 520 nm on a fluorescence microplate reader (FLx800; Biotec, Winoosk, VT) 1 h following the addition of substrate. Relative fluorescence units (RFU) were determined by subtracting background values (substrate-containing well without protease) from the raw fluorescence values, as described previously.[25] The dose-dependent FRET inhibition curves were fitted with a variable slope by using GraphPad Prism software (GraphPad, La Jolla, CA) in order to determine the IC_{50} values of the compounds. The expression and purification of the 3CLpro of MERS-CoV, as well as the FRET enzyme assays were performed as described previously.[17-18, 25]

Cell-based assay for antiviral activity. Compounds *2a* and *3a* were investigated for their antiviral activity against the replication of SARS-CoV-2. Briefly, confluent Vero E6 cells were inoculated with SARS-CoV-2 at 50-100 plaque forming units/well, and medium containing various concentrations of each compound and agar was applied to the cells. After 48-72 hr, plaques in each well were counted. The 50% effective concentration (EC_{50}) values were determined by GraphPad Prism software using a variable slope (GraphPad, La Jolla, CA).

Nonspecific cytotoxic effects/In vitro cytotoxicity. Confluent cells grown in 96-well plates were incubated with various concentrations (1 to 100 µM) of each compound for 72 h. Cell cytotoxicity was measured by a CytoTox 96 nonradioactive cytotoxicity assay kit (Promega, Madison, WI), and the CC_{50} values were calculated using a variable slope by GraphPad Prism software. The *in vitro* Safety Index was calculated by dividing the CC_{50} by the IC_{50}.

X-ray Crystallographic Studies

Crystallization and Data Collection. Purified SARS-2 3CL protease (SARS-2 3CLpro) in 100mM NaCl, 20mM Tris buffer, pH 8.0, was concentrated to 9.6 mg/mL (0.28 mM) for crystallization screening. All crystallization experiments were set up using an NT8 drop-setting robot (Formulatrix Inc.) and UVXPO MRC (Molecular Dimensions) sitting drop vapor diffusion plates at 18 °C. 100 nL of protein and 100 nL crystallization solution were dispensed and equilibrated against 50 µL of the latter. Stock solutions of the inhibitors (100 mM) were prepared in DMSO and the complexes were obtained by mixing 1 µL of the ligand (2 mM) with 49 µL (0.28 mM) of SARS-2 3CLpro and incubating on ice for 1 h.

Crystals were obtained in 1-2 days from the following conditions. *2a* and *3b*: Berkeley screen (Rigaku Reagents) condition C5 (20% (w/v) PEG 4000, 100 mM Tris pH 8.0), *2f*: Index HT screen (Hampton Research) condition H6 (20% (w/v) PEG 3350, 200 mM sodium formate), *2k*: Proplex HT screen (Molecular Dimensions) condition D7 (15% (w/v) PEG 6000, 100 mM sodium citrate pH 5.5), *3c* and *3d*: the Berkeley screen (Rigaku Reagents) condition D9 (20% (w/v) PEG 3350, 100 mM Bis-Tris pH 6.5, 100 mM ammonium phosphate dibasic, 5% (v/v) 2-propanol) and *3e*: Index HT screen (Hampton Research) condition C5 (15% (w/v) PEG 3350, 100 mM succinic acid pH 7.0). Samples were transferred to cryoprotectant solutions, prior to plunging in liquid nitrogen, composed of 80% crystallization solution and 20% (v/v) PEG 200 except for *3c* and *3d* for which 20% (v/v) ethylene glycol was used as the cryoprotectant. X-ray diffraction data were collected at the Advanced Photon Source IMCA-CAT beamline 17-ID except for the data for the complex with *3c* which were collected at the National Synchrotron Light Source II (NSLS-II) AMX beamline 17-ID-1.

Structure Solution and Refinement. Intensities were integrated using XDS[30-31] via Autoproc[32] and the Laue class analysis and data scaling were performed with Aimless.[33] Structure solution was conducted by molecular replacement with Phaser[34] using a previously determined structure of SARS-2 3CLpro (PDB 6XMK) as the search model. Structure refinement and manual model building were conducted with Phenix[35] and Coot[36], respectively. Disordered side chains were truncated to the point for which electron density could be observed. Structure validation was conducted with Molprobity[37] and structure analysis/figure preparation were carried out using the CCP4mg package.[38] Crystallographic data are provided in **Table S1**.

ASSOCIATED CONTENT

Supporting Information

The Supporting Information is available free of charge on the ACS Publications website.

Supplemental information (.docx)

Molecular formula strings – SMILES codes (.csv)

AUTHOR INFORMATION

Corresponding authors

*(W.C.G.) Phone: 316-978-7374. E-mail: bill.groutas@wichita.edu.

*(K-O.C.) Phone: 785-532-4039. E-mail: kchang@vet.ksu.edu

Notes

The authors declare no competing financial interest.

BioMolecular Structure (CBMS) is primarily supported by the National Institutes of Health, National Institute of General Medical Sciences (NIGMS) through a Center Core P30 Grant (P30GM133893), and by the DOE Office of Biological and Environmental Research (KP1605010).

ABBREVIATIONS USED

ORF, open reading frame; DSC, N,N'-disuccinimidyl carbonate; TEA, Triethyl amine; DMP, Dess-Martin periodinane; DTT, dithiothreitol; DMSO, dimethyl sulfoxide; MNV, murine norovirus; MOI, multiplicity of infection; CPE, cytopathic effects; $TCID_{50}$, the 50% tissue culture infectious dose; IC_{50}, the 50% inhibitory concentration in the enzyme assay; EC_{50}, the 50% effective concentration in cell culture; CC_{50}, 50% cytotoxic concentration in cell-based assays; GESAMT, general efficient structural alignment of macromolecular targets; RMSD, root mean square deviation; XDS, X-ray detector software; MME, monomethyl ether; PK, pharmacokinetics.

Accession Codes

Coordinates and structure factors for the following SARS2 3CLpro complexes with inhibitors were deposited to the Worldwide Protein Databank (wwPDB) with the accession codes: 7LKR (*2a*), 7LKS (*2f*), 7LKT (*2k*), 7LKU (*3b*), 7LKV (*3c*), 7LKW (*3d*) and 7LKX (*3e*). Authors will release the atomic coordinates upon article publication.

References

1. Perlman, S., Masters, P.S.; *Coronaviridae*: *The Viruses and Their Replication,* in Fields Virology: Emerging Viruses; Howley, P.M., Knipe, D.M., Whelan, S., Eds.; Wolters Kluwer: Wichita, 2020; Vol. 1, pp 410-448.

2. Hu, T.; Liu, Y.; Zhao, M.; Zhuang, Q.; Xu, L.; He, Q., A comparison of COVID-19, SARS and MERS. *PeerJ* **2020,** *8*, e9725.

3. Wu, F.; Zhao, S.; Yu, B.; Chen, Y.-M.; Wang, W.; Song, Z.-G.; Hu, Y.; Tao, Z.-W.; Tian, J.-H.; Pei, Y.-Y.; Yuan, M.-L.; Zhang, Y.-L.; Dai, F.-H.; Liu, Y.; Wang, Q.-M.; Zheng, J.-J.; Xu, L.; Holmes, E. C.; Zhang, Y.-Z. A new coronavirus associated with human respiratory disease in China. *Nature* **2020,** *579,* 265-269.

4. Dong, E.; Du, H.; Gardner, L., An interactive web-based dashboard to track COVID-19 in real time. *Lancet Infect. Dis.* **2020,** *20,* 533-534.

5. Ghosh, A. K.; Brindisi, M.; Shahabi, D.; Chapman, M. E.; Mesecar, A. D., Drug development and medicinal chemistry efforts toward SARS-Coronavirus and Covid-19 therapeutics. *Chem. Med. Chem.* **2020**, *15*, 907-932.

6. Gil, C.; Ginex, T.; Maestro, I.; Nozal, V.; Barrado-Gil, L.; Cuesta-Geijo, M. A.; Urquiza, J.; Ramírez, D.; Alonso, C.; Campillo, N. E., Martinez A., COVID-19: Drug targets and potential treatments. *J. Med. Chem.* **2020**, *63,* 12359-12386.

7. Sharma, A.; Tiwari, S.; Deb, M. K.; MARTY, J. L., Severe Acute Respiratory Syndrome Coronavirus-2 (SARS-CoV-2): A global pandemic and treatments strategies. *Intl J. Antimicrob. Agents* **2020**, *56,* 106054.

8. Cannalire, R.; Cerchia, C.; Beccari, A. R.; Di Leva, F. S.; Summa, V., Targeting SARS-CoV-2 proteases and polymerase for COVID-19 treatment: State of the art

and future opportunities. *J. Med. Chem.* [online early access]. DOI: 10.1021/acs.jmedchem.0c01140. Published online: Nov 13, 2020. https://doi.org/10.1021/acs.jmedchem.0c01140 (accessed Nov 13, 2020).

9. Ullrich, S.; Nitsche, C., The SARS-CoV-2 main protease as drug target. *Bioorg. Med. Chem. Lett.* **2020**, *30*, 127377.

10. Rut, W.; Lv, Z.; Zmudzinski, M.; Patchett, S.; Nayak, D.; Snipas, S. J.; El Oualid, F.; Huang, T. T.; Bekes, M.; Drag, M., Activity profiling and crystal structures of inhibitor-bound SARS-CoV-2 papain-like protease: A framework for anti–COVID-19 drug design. *Science Adv.* **2020,** *6,* eabd4596.

11. Jin, Z.; Du, X.; Xu, Y.; Deng, Y.; Liu, M.; Zhao, Y.; Zhang, B.; Li, X.; Zhang, L.; Peng, C., Duan, Y.; Yu, J.; Wang, L.; Yang, K.; Liu, F.; Jiang, R.; Yang, X.; You, T.; Liu, X.; Yang, X.; Bai, F.; Liu, H.; Liu, X.; Guddat, L.W.; Xu, W.; Xiao, G.; Qin, C.; Shi, Z.; Jiang, H.; Rao, Z.; Yang, H., Structure of M pro from SARS-CoV-2 and discovery of its inhibitors. *Nature* **2020**, *582,* 289-293.

12. Zhang, L.; Lin, D.; Sun, X.; Curth, U.; Drosten, C.; Sauerhering, L.; Becker, S.; Rox, K.; Hilgenfeld, R., Crystal structure of SARS-CoV-2 main protease provides a basis for design of improved α-ketoamide inhibitors. *Science* **2020,** *368,* 409-412.

13. Dai, W.; Zhang, B.; Jiang, X.-M.; Su, H.; Li, J.; Zhao, Y.; Xie, X.; Jin, Z.; Peng, J.; Liu, F., Li, C.; Li, Y.; Bai, F.; Wang, H.; Cheng, X.; Cen, X.; Hu, S.; Yang, X.; Wang, J,; Liu, X.; Xiao, G.; Jiang, H.; Rao, Z.; Zhang, L.-K.; Xu, Y.; Yang, H.; Liu, H. Structure-based design of antiviral drug candidates targeting the SARS-CoV-2 main protease. *Science* **2020,** *368,* 1331-1335.

14. Hoffman, R. L.; Kania, R. S.; Brothers, M. A.; Davies, J. F.; Ferre, R. A.; Gajiwala, K. S.; He, M.; Hogan, R. J.; Kozminski, K.; LI, L. Y.; Lockner, J. W.; Lou, J.; Marra, M. T.; Mitchell Jr, L.J.; Murray, B. W.; Nieman, J.A.; Noell, S.; Planken, S. P.; Rowe, T.; Ryan, K.; Smith III, G.J.; Solowiej, J. E.; Steppan. C. M.; Taggart, B. Discovery of ketone-based covalent inhibitors of coronavirus 3CL proteases for the potential therapeutic treatment of COVID-19. *J. Med. Chem.* **2020**, *63*, 12725-12747.

15. Qiao, J.; Li, Y-S.; Zeng, R.; Liu, F-L.; Luo, R-H.; Huang C.; Wang, Y-F.; Zhang, J.; Quan, B.; Shen, C.; Mao, X,; Liu, X.; Sun, W.; Yang, W.; Ni, X.; Wang, K.; Xu, L.; Duan, Z-L.; Zou, Q-C.; Zhang, H-L.; Qu, W.; Long, Y-H-P.; Li, M-H.; Yang, R-C.; Liu, X.; You, J.; Zhou, Y.; Yao, R.; Li, W-P.; Liu, J-M.; Chen, P.; Liu, Y.; Lin, G-F.; Yang, X.; Zou, J.; Li, L.; Hu, Y.; Lu, G-W.; Li, W-M.; Wei, Y-Q.; Zheng, Y-T.; Lei, J.; Yang, S., SARS-CoV-2 M^{pro} inhibitors with antiviral activity in a transgenic mouse model. *Science* **2021**, *371*, 1374-1378.

16. Schechter, I., Reprint of "on the size of the active site in proteases. I. Papain". *Biochem. Biophys. Res. Com.* **2012,** *425* , 497-502. The nomenclature used is that of Schechter, I. and Berger, A., where the residues on the N-terminus side of the peptide bond that is cleaved are designated as P_1-P_n and those on the C-terminus side are designated P_1-P_1'. The corresponding active site subsites are designated S_1-S_n and S_1-S_n'. S_1 is the primary substrate specificity subsite and P_1-P_1' is the scissile bond.

17. Rathnayake, A. D.; Zheng, J.; Kim, Y.; Perera, K. D.; Mackin, S.; Meyerholz, D. K.; Kashipathy, M. M.; Battaile, K. P.; Lovell, S.; Perlman, S., 3C-like protease

inhibitors block coronavirus replication in vitro and improve survival in MERS-CoV– infected mice. *Science Transl. Med.* **2020,** *12* :eabc5332.

18. Kim, Y.; Liu, H.; Galasiti Kankanamalage, A. C.; Weerasekara, S.; Hua, D. H.; Groutas, W. C.; Chang, K.-O.; Pedersen, N. C., Reversal of the progression of fatal coronavirus infection in cats by a broad-spectrum coronavirus protease inhibitor. *PLoS Pathog.* **2016,** *12,* e1005531.

19. Pedersen, N. C.; Kim, Y.; Liu, H.; Galasiti Kankanamalage, A. C.; Eckstrand, C.; Groutas, W. C.; Bannasch, M.; Meadows, J. M.; Chang, K.-O., Efficacy of a 3C-like protease inhibitor in treating various forms of acquired feline infectious peritonitis. *J. Feline Med. Surg.* **2018,** *20,* 378-392.

20. Pirali, T.; Serafini, M.; Cargnin, S.; Genazzani, A. A., Applications of deuterium in medicinal chemistry. *J. Med. Chem.* **2019,** *62*, 5276-5297.

21. Timmins, G. S. Deuterated drugs: updates and obviousness analysis. *Expert Opin Ther. Pat.* **2017**, *27*, 1353-1361.

22. Liu, J. F.; A decade of deuteration in medicinal chemistry. *Ann. Rep. Med. Chem.* **2017**, *50*, 519-542.

23. Ghosh, A. K.; Duong, T. T.; McKee, S. P.; Thompson, W. J., N, N'-Disuccinimidyl carbonate: A useful reagent for alkoxycarbonylation of amines. *Tetrahedron Lett.* **1992,** *33,* 2781-2784.

24. Kjell, D. P.; Slattery, B. J.; Semo, M. J., A novel, nonaqueous method for regeneration of aldehydes from bisulfite adducts. *J. Org. Chem.* **1999,** *64,* 5722-5724.

25. Kim, Y.; Lovell, S.; Tiew, K.-C.; Mandadapu, S. R.; Alliston, K. R.; Battaile, K. P.; Groutas, W. C.; Chang, K.-O., Broad-spectrum antivirals against 3C or 3C-like proteases of picornaviruses, noroviruses, and coronaviruses. *J. Virol.* **2012,** *86*, 11754-11762.

26. Gampe, C.; Verma, V. A. Curse or cure? A perspective on the developability of aldehydes as active pharmaceutical ingredients. *J. Med. Chem.* **2020**, *63*, 14357-14381.

27. Cargnin, S.; Serafini, M.; Pirali, T. A primer of deuteration in drug design. *Future Med. Chem.* **2019**, *11*, 2039-2042.

28. Meanwell, N. A. Synopsis of some recent tactical application of bioisosteres in drug design. *J. Med. Chem.* **2011**, *54*, 2529-2591.

29. Chessari, G.; Hardcastle, I. R.; Ahn, J. S.; Anil, B.; Anscombe, E.; Bawn, R. H.; Bevan, L. D.; Blackburn, T. J.; Buck, I.; Cano, C.; Carbain, B.; Castro, J.; Cons, B.; Cully, S. J. Endicott, J. A.; Fazal, L.; Golding, B. T.; Griffin, R. J.; Haggerty, K.; Harnor, S. J.; Hearn, K.; Hobson, S.; Holvey, R. S.; Howard, S.; Jennings, C. E.; Johnson, C. N.; Lunec, J.; Miller, D. C.; Newell, D. R., Noble, M. E. M.; Reeks, J.; Revill, C. H.; Riedinger, C.; Denis, J. D. St.; Tamanini, E.; Thomas, H.; Thompson, N. T.; Vinkovic, M.; Wedge, S. R.; Williams, P. A.; Wilsher, N. E.; Zhang, B.; Zhao, Y., Structure-based design of potent and orally active isoindolinone inhibitors of MDM2-p53 protein-protein interaction. *J. Med. Chem.* **2021**, *64*, 4071-4088.

30. Kabsch, W., Automatic indexing of rotation diffraction patterns. *J. Applied Crystallogr.* **1988,** *21,* 67-72.

31. Kabsch, W., XDS. *Acta Crystallogr. D* **2010,** *66*, 125-132.

32. Vonrhein, C.; Flensburg, C.; Keller, P.; Sharff, A.; Smart, O.; Paciorek, W.; Womack, T.; Bricogne, G., Data processing and analysis with the autoPROC toolbox. *Acta Crystallogr. Section D: Biolog. Crystallogr.* **2011,** *67,* 293-302.

33. Evans, P. R., An introduction to data reduction: space-group determination, scaling and intensity statistics. *Acta Crystallogr. Section D: Biolog. Crystallogr.* **2011,** *67,* 282-292.

34. McCoy, A. J.; Grosse-Kunstleve, R. W.; Adams, P. D.; Winn, M. D.; Storoni, L. C.; Read, R. J., Phaser crystallographic software. *J. Appl. Crystallogr.* **2007,** *40,* 658-674.

35. Adams, P. D.; Afonine, P. V.; Bunkóczi, G.; Chen, V. B.; Davis, I. W.; Echols, N.; Headd, J. J.; Hung, L.-W.; Kapral, G. J.; Grosse-Kunstleve, R. W., PHENIX: a comprehensive Python-based system for macromolecular structure solution. *Acta Crystallogr. Section D: Biolog. Crystallogr.* **2010,** *66,* 213-221.

36. Emsley, P.; Lohkamp, B.; Scott, W. G.; Cowtan, K., Features and development of Coot. *Acta Crystallogr. Section D: Biolog. Crystallogr.* **2010,** *66,* 486-501.

37. Chen, V. B.; Arendall, W. B.; Headd, J. J.; Keedy, D. A.; Immormino, R. M.; Kapral, G. J.; Murray, L. W.; Richardson, J. S.; Richardson, D. C., MolProbity: all-atom structure validation for macromolecular crystallography. *Acta Crystallogr. Section D: Biolog. Crystallogr.* **2010,** *66,* 12-21.

38. Potterton, L.; McNicholas, S.; Krissinel, E.; Gruber, J.; Cowtan, K.; Emsley, P.; Murshudov, G. N.; Cohen, S.; Perrakis, A.; Noble, M., Developments in the CCP4 molecular-graphics project. *Acta Crystallogr. Section D: Biolog. Crystallogr.* **2004,** *60*, 2288-2294.

39. Evans, P. Scaling and assessment of data quality, *Acta Crystallogr. Sect D: Biol. Crystallogr.* **2006,** *62*, 72-82.

40. Diederichs, K.; Karplus, P. A. Improved R-factors for diffraction data analysis in macromolecular crystallography, *Nat. Struct. Biol.* **1997,** *4,* 269-275.

41. Weiss, M. S. Global indicators of X-ray data quality, *J. Appl. Crystallogr.* **2001,** *34* 130-135.

42. Karplus, P. A.; Diederichs, K. Linking crystallographic model and data quality, *Science* **2012,** *336,* 1030-1033.

43. Evans, P. Biochemistry. Resolving some old problems in protein crystallography, *Science* **2012,** *336,* 986-987.

Table of Contents Graphic